

# **Compressed Sensing: Single Pixel Imaging in Short-Wave Infrared Spectrum**

**Examensarbete**

TQET33

Andreas Brorsson, Andbr981, (911023-1215)

Linköping, 2017

# 1 Introduction

The development and research of compressed sensing applied to a single pixel camera (SPC) is a relative new area in signal processing with the first functioning camera architecture in 2006. Since then numerous improvements and methods have been proposed how to capture images. In this section a introduction to the SPC architecture and a brief introduction of compressed imaging is presented followed by the aim, research questions and thesis outline.

## 1.1 Background

Compressed sensing (CS) allows reconstruction of a sparse signal being sampled with far fewer samples required to fulfill the sampling theorem. Swedish Defence Research Agency (FOI) became interested in the subject some years ago and tests potential applications. One of the potential applications are a camera with a single pixel which can reconstruct a scene, therefore FOI built a SPC platform in the short-wave infrared (SWIR) spectrum for the purpose to study and evaluate this kind of system.

The SWIR spectrum is electromagnetic radiation with wavelengths between 700 - 2500 nm and SWIR cameras can therefore capture images illuminated by the sun, moon, star light and airglow thus works both by day and night. SWIR light can to some extent pass through smoke and fog which makes it robust camera for day and night applications. Some camouflage that is hard to spot in visual spectrum is visible in the SWIR spectrum. The system used in this master's thesis uses a digital micromirror array (DMD) to sample the light from the scene. The system will sample less single pixel measurements than the number of pixels in the reconstructed image with the drawback that it has to capture each measurement in consecutive order instead of all at the same time.

## 1.2 Compressive sensing & imaging

Compressive sensing is a new sampling strategy which reconstructs a compressible or sparse signal by finding solution to undetermined linear system where the number of measurements  $M$  is less than the number of data points  $N$  in signal. Two constraints need to be fulfilled to apply compressed sensing sampling: the sampled signal needs to be spares in some basis e.g. Fourier or gradient, the second condition is that the measurement matrix must be incoherent with the sparse transform. The characteristic undetermined linear system in CS is defined as  $\mathbf{y} = \Phi\mathbf{x}$  where  $\mathbf{y}$  contains the measurements from the measurement matrix  $\Phi$  sensing the signal  $\mathbf{x}$ . In figure 1 such linear equation system is shown.

$$\begin{matrix} \mathbf{y} \\ \begin{matrix} y_1 \\ y_2 \\ y_3 \\ \vdots \\ y_M \end{matrix} \end{matrix} = \boxed{\Phi} \quad \begin{matrix} \mathbf{x} \\ \begin{matrix} x_1 \\ x_2 \\ x_3 \\ x_4 \\ \vdots \\ \vdots \\ x_N \end{matrix} \end{matrix}$$

The diagram illustrates the linear equation system  $\mathbf{y} = \Phi\mathbf{x}$ . On the left, a vertical vector  $\mathbf{y}$  is shown with elements  $y_1, y_2, y_3, \dots, y_M$ . An equals sign follows. To the right of the equals sign is a large rectangular box labeled  $\Phi$ , which represents the measurement matrix. This matrix has  $M$  rows, corresponding to the elements of  $\mathbf{y}$ , and  $N$  columns, corresponding to the elements of  $\mathbf{x}$ . The individual entries of the matrix are labeled  $\Phi_1, \Phi_2, \Phi_3, \dots, \Phi_M$ . To the right of the matrix is another vertical vector  $\mathbf{x}$  with elements  $x_1, x_2, x_3, x_4, \dots, x_N$ .

Figure 1: CS undetermined linear system

Scientists at Rice university in Texas, USA realized that the new method could be used to create a new camera architecture with a single photo diode in the sensor, the single pixel camera was born and thus a new sub field of compressed sensing was created called compressive imaging.

To be able to apply CS to imaging in the first place the constraints in CS needs to hold for images as well. The first requirement is that the signal needs to be compressible or sparse in some basis which natural images is known to be because they can be compressed using for example JPEG (Discrete cosine transform), JPEG2000 (Wavelet). The second constraint is that the measurement matrix must be incoherent with the sparse transform which for example i.i.d random distribution or some structure with the same property as i.i.d random distribution.

### 1.3 System architecture

The SPC in this master's thesis was designed with reflecting telescope optics to act as a lens to focus the scene. As seen in figure 2 light from the scene enters through the aperture in the camera where the primary mirror focus the light the via the secondary mirror onto the DMD. To this point, the SPC works like a conventional camera with a DMD where the image sensor would be placed in the convectional camera. The SPC has an DMD in the focal point which resemble an image sensor but instead of photo diodes for each pixel there is a tiny mirror which individually can either reflect light 12 degrees to the right or left as seen in figure 2. The incoming focused light can ether be dumped or it can be reflected into the single pixel SWIR detector through an lens.

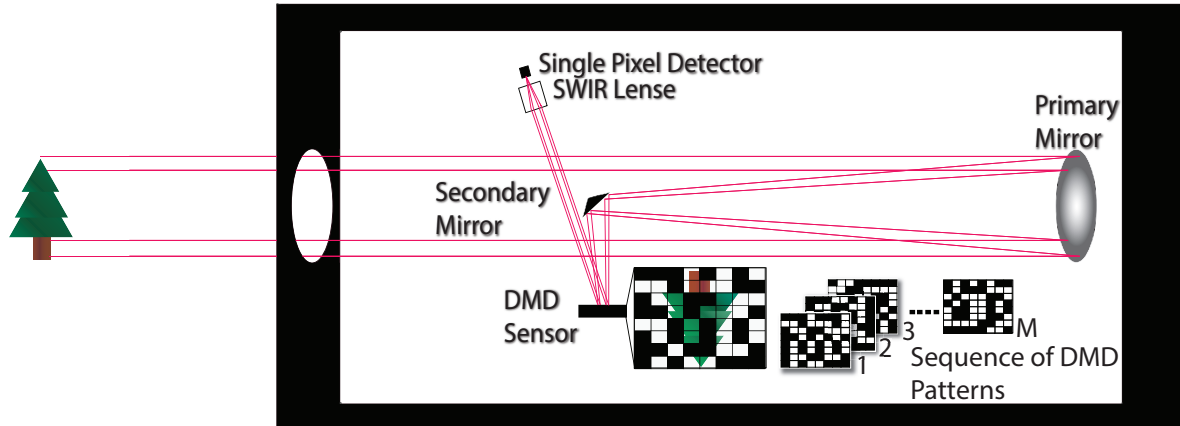


Figure 2: System overview

To connect the architecture with the math from CS it can be interpreted as, the light from the scene which is focused on the DMD is the desired signal  $\mathbf{x}$ , the image. The DMD can individually set each mirror the ether direct the light from each 'pixel' to the single pixel sensor or dump the light i.e a spatial light modulator (SLM). The DMD sets a pattern of pixel of intress which is a measurement matrix  $\Phi_m$  to be summarized in the single pixel sensor  $y_m$  as a measurement. One measurement is the inner product of a measurement matrix and the signal,  $\Phi_m \times x = y_m$ . To complete a full measurement the process is repeated with different measurement matrices set on the DMD to the full undetermined linear system  $\mathbf{y} = \Phi\mathbf{x}$ .

### 1.4 Measurement matrix & reconstruction

How is the measurement matrix chosen? As told before the measurement matrix needs to be incoherent with the sparse transform and the DMD can only direct the light or not which mathematically is ether a zero or a one. The research tells that for example a i.i.d. Gaussian distribution with equal probability of a zero or one will with high probability be incoherent with a natural image scene. But how about the first constraint that the signal  $\mathbf{x}$  needs to be sparse or compressible in some basis? Often natural images is not sparse in the spatial domain unless the scene

is for example the night sky, well a good property of CS that the scene can be transformed to an other basis like this,

$$\mathbf{y} = \Phi \mathbf{x} \Leftrightarrow \mathbf{y} = \Phi \Psi \Theta, \quad (1)$$

where  $\Psi$  is a sparsifying basis for example to the DCT or Wavelet basis. And  $\Theta$  is the coefficients vector which is more sparse then the spatial coefficient vector  $\mathbf{x}$ . And the transformation will not compromise the incoherence between the reconstruction matrix  $A = \Psi \Phi$  and the coefficients  $\Theta$  in the new basis. This means that the signal  $\mathbf{x}$  will be reconstructed with optimization in a more sparse basis  $\Theta$  and then transformed back to the spatial domain.

What is special about CS is not just how the problem is presented but also how to solve it. It is known that an undetermined linear system has infinite many solution so how does the signal get recovered? CS exploit the characteristics of the signal  $x$  which is known to be sparse in some basis. With for example  $\ell_1$  optimization,

$$\hat{\Theta} = \arg \min \|\Theta\|_{\ell_1} \text{ subject to } \Phi \Psi \Theta = y, \quad (2)$$

which means that  $\ell_1$  optimization minimizes the non zero elements of  $\Theta$  and can exactly reconstruct a K-spares vector or approximate a compressible vector. The exact recovery can be accomplished with high probability using  $M \geq \mathcal{O}(K \log(N/K))$  measurements. This is why CS is powerful, it enables sub-Nyquist measurements with exact recovery in the noiseless case which can be approximated in real applications.

In the compressed imaging case where noise is present an other optimization algorithm has shown to be more successful at recovering images: total variation. Total variation regularization minimizes the magnitude of the gradient in the image and doing so it preserve edges and piece-wise constant structure in the image which is desired.

## 1.5 Motivation

Why would a SPC be beneficial to a conventional camera? The SPC has more components and several measurements have to be made over time while a regular camera measures all pixels on the sensor at the same time, and the reconstruction shifts burden to the processor. There are two major reasons why a SPC is of interest, it is not to compete with the conventional cameras in the visual spectrum where cameras in all price ranges and quality already exist and are relative cheap to build. The focus lies in more exotic spectrum of light like SWIR or Terahertz (X-ray) wavelengths where the image sensors are hard to build which brings up cost and the ability to create high resolution sensors. With CS and the SPC architecture manufacturing cost can be significantly reduced while the image resolution increases. For example a state of the art SWIR camera cost about half a million SEK which can be reduced by a factor of 100 with a SPC with the same resolution.

## 1.6 Aim

What image quality can be achieved in natural images captured with a single pixel camera in daylight using state of the art methods?

## 1.7 Research questions

- How can the quality of images reconstructed by CS or a SPC be evaluated?
- What is the state of the art method to capture and reconstruct images using a SPC architecture?
- What image quality is achieved using state of the art methods applied to the SPC?

Add hypothesis that dynamics in scene can be suppressed?

## 1.8 Limitations

- The hardware rig provided by FOI
- 

## 1.9 Thesis outline

## 2 Related work

In this section important, relevant and fundamental articles to this master's thesis is presented each with a summary. The articles covers compressed sensing theory applied to compressed imaging, SPC architecture and how to evaluate the images i.e. the fundamental source of information on how to build a state of the art SPC system and how to evaluate its performance.

### 2.1 Compressive sensing

- [1], [2] Two books which thoroughly presents the topic sparse and redundant representation and sparse modeling. The fundamental principles and constraints that needs to be fulfilled in CS. The books presents different minimization algorithms and how to implement them.
- In [3] David L. Donoho proposed the framework of compressed sensing and its application to images.

### 2.2 Compressive imaging

- [4] "Single-Pixel Imaging via Compressive Sampling"
- [5] "Compressed sensing for practical optical imaging systems: a tutorial"
- [6] "A New compressive imaging camera architecture using Optical-Domain Compression"
- [7] "An architechture for compressive imaging"
- [8] "A high resolution SWIR camera via compressed sensing"
- [5] "Compressive Sensing: From Theory to Applications, A survey"
- [9] "Compressed Sensing for 3D Laser Radar"
- [10] "Multi image super resolution using compressed sensing"
- [11] An article presenting the setup used in this master's thesis with a proof of concept that the SPC setup works.

#### 2.2.1 Measurement matrix & reconstruction

- [12] Chengbo Li:s master's thesis "An Efficient Algorithm For Total Variation Regularization with Applications to the Single Pixel Camera and Compressive Sensing" describes his new total variation algorithm Li constructed which solve the CS problem. The algorithm is faster and produces better results for images than previous popular algorithms.
- [13]–[15] Fast and Efficient Compressive Sensing Using Structurally Random Matrices (SRM). The articles describes why and how to implement SRM, in these articles the Hadamard or DCT matrices is proposed to replace the i.i.d random matrix. With SRM the reconstruction time is reduced by replacing matrix multiplication with fast transforms. In addition to improved reconstruction time the new method does not need to store the measurement matrix in memory which enables reconstruction of high resolution images.
- [16] "An Improved Hadamard Measurement Matrix Based on Walsh Code For Compressive Sensing" Shows that sequency-ordered Walsh Hadamard matrix gives better reconstruction then the Hadamard matrix with the same benefits of using the Hadamard matrix. The resulting reconstructed image has near optimal reconstruction performance.
- [17] Proof that permuted Walsh Hadamard measurement matrices fulfills RIP.

## 2.3 Evaluation

- Al Boviks book the essential guide to image processing [18] contains the majority of fundamental image processing techniques and measurements. Two image quality metrics of interest is PSNR and SSIM which can be used when a reference image is available.
- [19] "No-Reference Image Quality Assessment in the Spatial Domain" is the article describing the blind/referenceless image spatial quality evaluator (BRISQUE). The BRISQUE algorithm evaluates image quality and "naturalness" based on statistics in the image. BRISQUE is used when there is no reference image available therefore can be used to evaluate images produced by the SPC.

## 2.4 Analysis

### 3 Method

New method introduction depending on how the disposition will be in the final form

In order to answer the research questions stated in section 1.7 a state of the art SPC, experiments and evaluation methods needs to be set up. In this section the SPC hardware and image sensing and reconstruction scheme is described.

#### 3.1 Single pixel camera architecture & hardware

FOI designed the SWIR SPC platform using a DMD, a Newtonian telescope and a single pixel SWIR detector. The system also has a reference camera in the visual spectrum which can capture images if all micro mirrors in the DMD are turned away from the single pixel sensor and towards the reference camera, it can also be used to check that the patterns are displayed correct on the DMD.

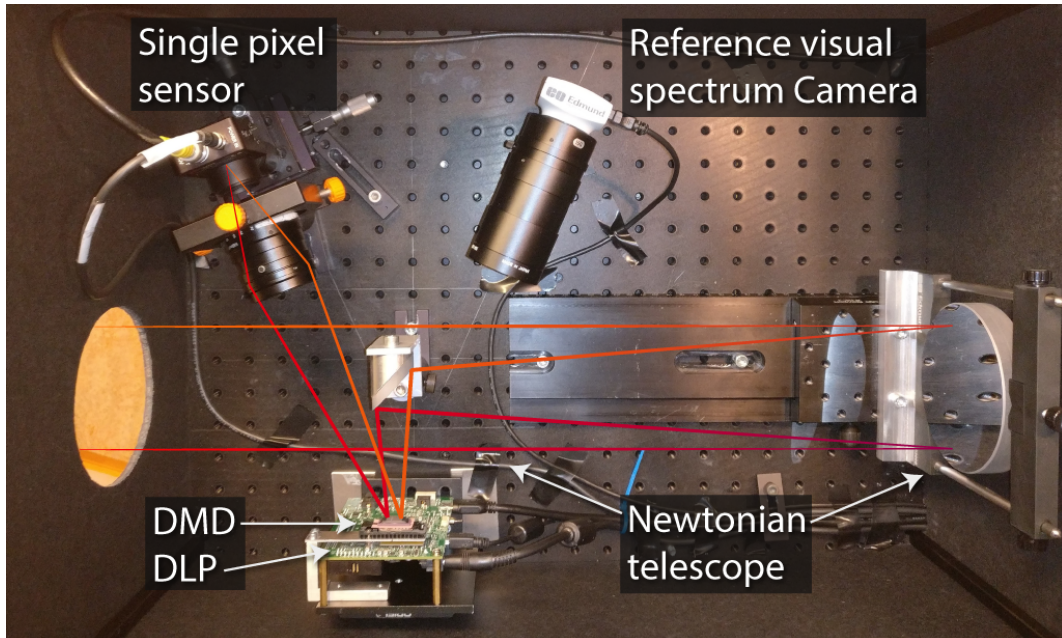


Figure 3: Single pixel imaging system (SPIS), adopted from [11].

As seen in figure 3 light from the scene is focused by the Newtonian telescope and reflected onto the DMD. The mirrors on the DMD can turned individually either into the single pixel sensor or the reference camera. The DMD acts as a Spatial Light Modulator (SLM) and reflects different patterns which is 'summed up' in the single pixel sensor as an intensity. The reconstructed image from the system will have the same resolution as the DMD patterns. The DLP is the DMD control unit which controls which patterns are displayed on the DMD either by reading images from memory or the video port.

##### 3.1.1 Newtonian telescope

A Newtonian telescope is a reflecting telescope, using a concave primary mirror and a flat diagonal secondary mirror, see figure 3. In this set-up the telescope act as a lens focusing the scene onto the DMD. The motivation to use a Newtonian telescope instead of a lens system is partly that chromatic aberration is eliminated and partly that a reflective optical system works over a greater range of wavelengths that includes SWIR, near infrared (NIR) and the visible spectrum.

### 3.1.2 DLP and DMD

The DMD (Texas Instruments DLP4500NIR) is a matrix of micro mirrors that can be individually tilted  $\pm 12^\circ$  and reflects wavelengths in the range 700-2500 nm. The DMD is controlled by the DLP (DLP LightCrafter 4500) which can be controlled either by video port (HDMI) or by the internal flash memory. The internal memory can theoretically be faster than the video port but due to constraints in both memory and memory bandwidth the fastest measurement matrix rate gets stuck at 270 – 300 Hz. The video port can be operated at 120 Hz and display one bit plane at the time from a 24 bit signal, which gives a maximum measurement matrix rate at  $120 \times 24 = 2880$  Hz, but in the current configuration only 60 Hz frame rate was achieved giving a measurement matrix rate at 1440 Hz. At this rate with the number of measurements relative to number of pixels in reconstructed image between 20% – 30% a  $256 \times 256$  pixel images data would be acquired in 9 – 13 seconds and for a  $512 \times 512$  pixel image 36 – 53 seconds. To control the DMD the software 'DLP LightCrafter 4500 Control Software' is used.

The DMD in the setup is constructed with a diamond shaped pattern instead of a regular square grid which is used in regular camera image sensors. The diamond shape causes the index of each mirror to be skewed against what a normal grid would look like. As seen in figure 4 the indexes of the mirrors column is two mirror column arrays wide while a row is a single row.

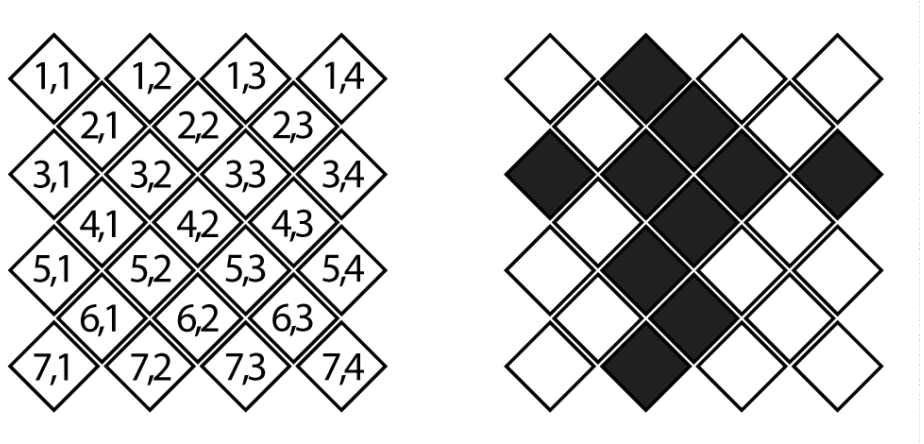


Figure 4: DMD matrix, left shows each tiles index and right shows second row and second column in black.

Because the reconstruction algorithm and measurement matrix needs to be a square matrix with the side length with a power of 2 the resulting images ratio would be 2 to 1 while the image should have the ratio 1 to 1. The resulting image would need to be transformed into the real ratio where information potentially gets lost. Therefore the index of mirrors was changed so that each 'pixel' gets two mirrors as seen in figure 5. This will result in rows and columns gets equal amount of space and the aspect ratio will be preserved to 1 to 1.



Figure 5: DMD matrix, left shows each tiles index and right shows third row and third column in black.

Connect the DMD to CS and the physical aspect (every mirror is an pixel). I:I:D gaussian with DMD only can take values 1,0 gives 50% evenly distributed pixels measurements for every measurement matrix which looks something like figure 6.



Figure 6: A typical measurement matrix presented on the DMD with the resolution  $256 \times 256$  pixels.

### 3.1.3 Lens

The lens mounted on the single pixel sensor is an 50mm SWIR Fixed Focal Length Lens with an variable appature from f1.4 designed for wavelengths ranging from the 800 nm in the visual spectrum to 2000 nm in the SWIR spectrum. [20]

### 3.1.4 Single pixel sensor

The single pixel sensor is a Thorlabs PDA20C/M and is sensitive in wavelength range 800-1700 nm which is beyond the visual spectrum (390-700 nm). The sensor outputs an analog signal in volt which the sampler converts to a discret value. [21]

### 3.1.5 Signal spectrum

All components characteristics assembled the wavelengths that pass through the system and measured in the single pixel sensor is between 800-1700 nm.

## 3.2 Compressive imaging

Write introduction to CS, create some intuition

The single pixel sensor captures a scene by measuring the light intensity focused into the detector reflected from the DMD matrix. The DMD sensing matrix changes to obtain new measurements,  $M$  unique sensing matrix measurements is captured to reconstruct an image with  $N$  pixels. Each sensing matrix index is encoded either by a one or a zero (turning the mirror onto or away from the sensor). The compressive imaging sampling model is defined as

$$\mathbf{y} = \Phi \mathbf{x} + \epsilon, \quad (3)$$

,  $\mathbf{x}_{N \times 1}$  is the signal (image) with  $N$  samples (pixels),  $\mathbf{y}_{M \times 1}$  is the vector with  $M$  measurements,  $\Phi_{M \times N}$  is the measurements matrix (each unique sensing matrix  $\Phi_{1 \times N}$  as a row vector) and  $\epsilon$  is the noise. In conventional sampling the number of measurements  $M$  needs to be at least equal to the number of samples  $N$  to recover the signal but CS states that  $M$  can be relatively small compared to  $N$  given how compressible the signal is. The signal  $\mathbf{x}$  can be represented as

$$\Psi \theta = \mathbf{x}, \quad (4)$$

where,  $\Psi_{N \times N}$  is some basis matrix and  $\theta_{N \times 1}$  is the coefficients where  $\theta$  is  $K$ -sparse.  $K$ -sparse means that the signal  $\mathbf{x}$  has  $K$  non zero elements in basis  $\Psi$ ,  $\|\theta\|_0 = K$ . Given equation 4, equation 3 can be expand to

$$\mathbf{y} = \Phi \mathbf{x} + \epsilon = \Phi \Psi \theta + \epsilon = \mathbf{A} \theta + \epsilon, \quad (5)$$

where,  $\mathbf{A}_{M \times N} = \Phi \Psi$  is the reconstruction matrix. The last statement is what makes CS powerful, a signal which is not sparse can be sampled with measurement matrix  $\Phi$  and then reconstructed with reconstruction matrix  $\mathbf{A}$  in a basis where  $\mathbf{x}$  is sparse or compressible. [1]

Noise does not effect the measurement very much because half the intensity from the image is measured in one pixel sensor bumping the signal to noise ratio from a conv camera where each pixel has some noise half the pixels share that noise making SPC very robust to noise even in low light situations.

## 3.3 Measurement matrix & Restricted isometry property (RIP)

Introduce the topic.

In the noiseless case exact recovery of the image  $\mathbf{x}$  is achievable if RIP holds for the reconstruction matrix  $\Phi \Rightarrow \Phi \Psi = \mathbf{A}$ , the constraint is defined as,

$$(1 - \delta_K) \|\mathbf{x}\|_{\ell_2}^2 \leq \|\mathbf{A} \mathbf{x}\|_{\ell_2}^2 \leq (1 + \delta_K) \|\mathbf{x}\|_{\ell_2}^2, \quad (6)$$

where  $\delta_K \in [0, 1)$  is the smallest constant to satisfy RIP for a  $K$ -sparse signal  $\mathbf{x}$ . To determine a sampling matrix is a NP-hard problem (which means that there are no feasible way of creating a optimal reconstruction matrix) and generally  $\mathbf{x}$  is not known and varies which means that there are no general optimal reconstruction matrices for natural images. The solution is to find a general

reconstruction matrix that satisfies RIP with high probability. The solution which also should be incoherent with the base matrix  $\Psi$  is to construct the measurement matrix using a i.i.d random distribution which gives  $\delta_K \ll 1$  with high probability. Using random measurement matrices the number of measurements needed to satisfy RIP with high probability is  $M \geq O(K \log(N/K)) \ll N$ . [2], [3]

The problem using random matrices is that they need to be stored in memory for the reconstruction algorithm, when the image resolution is increased the measurement matrix increases exponentially. For images with resolution of  $512 \times 512$  and larger the data gets infeasible for a normal computer to handle. Fortunately using fast transforms in the reconstruction algorithm can exclude using vector multiplication resulting in faster reconstruction and the need to store the measurement matrix in memory. But in order to do so special measurement matrices are used, in this master's thesis the sequency ordered Walsh Hadamard measurement matrix will be used with the TVAL3 reconstruction algorithm described in section 3.4.1.

### 3.3.1 Sequency ordered Walsh Hadamard measurement matrix

Besides from eliminating the need to store the measuring matrix for reconstruction the sequency ordered Walsh Hadamard (SOWH) matrix can be generated when sent to the DMD eliminating the need to store the matrix at all. SOWH has the same characteristics and properties of an i.i.d random matrix and therefore also fulfills the RIP condition with high probability and research has shown that there is no significant loss in recovery of the signal relative i.i.d random measurement matrix [16]. An other property of SOHW is that it only contains -1 and 1 which easily be converted to 0 and 1 when sent to the DMD.

The naturally ordered Hadamard matrix of dimension  $2^k$ ,  $k \in \mathbb{N}$  are constructed by the recursive formula

$$H_0 = 1, \quad (7)$$

$$H_1 = \begin{bmatrix} 1 & 1 \\ 1 & -1 \end{bmatrix}, \quad (8)$$

and in general,

$$H_k = \begin{bmatrix} H_{k-1} & H_{k-1} \\ H_{k-1} & -H_{k-1} \end{bmatrix} = H_1 \oplus H_{k-1} \quad (9)$$

where  $\oplus$  denotes the Kronecker product. To construct the sequency ordered Walsh Hadamard matrix from the naturally ordered Hadamard matrix three steps is required:

- Convert row index to binary.
- Convert the binary row index to gray code.
- Apply bit reverse on the gray code index.

then order the rows after the bit reverse to obtain the sequency ordered Walsh Hadamard matrix.

$n_H$	0	1	2	3
Binary	00	01	10	11
Gray code	00	01	11	10
Bit-reverse	00	10	11	01
$n_W$	0	2	3	1

Table 1: How to convert a naturally ordered Hadamard matrix to a sequency ordered Walsh Hadamard matrix by shifting row with index  $n_W$  to  $n_H$

for example

$$H_2 = \begin{bmatrix} 1 & 1 & 1 & 1 \\ 1 & -1 & 1 & -1 \\ 1 & 1 & -1 & -1 \\ 1 & -1 & -1 & 1 \end{bmatrix} \Rightarrow W_2 = \begin{bmatrix} 1 & 1 & 1 & 1 \\ 1 & 1 & -1 & -1 \\ 1 & -1 & -1 & 1 \\ 1 & -1 & 1 & -1 \end{bmatrix}. \quad (10)$$

To use the sequency ordered Walsh Hadamard matrix as an measurement matrix the fist row is omitted, permutations to the columns is performed,  $M$  rows are choosen at random and the indices with a  $-1$  is shifted to 0. This last step is required to convert the measurement matrix so it gets the characteristics of an i.i.d random matrix and thus fulfill the RIP condition [14], [17], [22]. How the matrix was permuted and which rows was choosen i which order is stored so the reconstruction algorithm can use that information. [12], [14], [16].

permutation is not nessesaray?

### 3.4 Reconstruction method

To reconstruct the image  $\mathbf{x}$  the sparest set of coefficients in  $\theta$  is desired. The optimal approach to find these coefficients would be to use  $\ell_0$  minimization

$$\hat{\theta} = \arg \min \|\theta\|_0 \text{ subject to } \mathbf{y} = \mathbf{A}\theta. \quad (11)$$

Simply minimizing nonzero indices  $\theta$  in the sparsitfying basis  $\Psi$ , but this problem is known to be NP-hard. A better approach is the  $\ell_1$  minimization, for example Basis Pursuit denoise (BPDN),

$$\hat{\theta} = \arg \min \|\theta\|_1 \text{ subject to } \|\mathbf{y} - \mathbf{A}\theta\|_2 < \epsilon. \quad (12)$$

In 2006 Donoho [3] for the fist time guarantied theoretical  $\ell_0/\ell_1$  equivalence which holds in the CS case, which means using a  $\ell_1$  minimizer is guaranteed to find the sparsest solution in polynomial time in the noiseless case which can be approximated in the noisy and compressible signal case. The drawback with the  $\ell_1$  minimizer is that it require more measurements than the optimal case with  $\ell_0$  but it is still  $M \ll N$ . Since 2006 many more types of optimization algorithms has evolved which solves the problem with different methods but with the same goal: finding the largest most significant coefficients of  $\theta$ . [3], [4], [6]

#### 3.4.1 Total variation: TVAL3

The reconstruction algorithm that was chosen in this Master's thesis was a total variation regularization algorithm. Natural images often contains sharp edges and piecewise smooth areas which the TV regularization algorithm is good at preserving. The main difference between TV an other reconstruction algorithms is that TV considers the gradient of signal sparse instead of the signal, thus finding the sparsest gradient. The TV optimization problem in TVAL3 is defined as

$$\min_{\mathbf{x}} \sum_i \|D_i \mathbf{x}\|, \text{ subject to } \Phi \mathbf{x} = y, \mathbf{x} \geq 0, \quad (13)$$

where  $D_i \mathbf{x}$  is the discrete gradient of  $\mathbf{x}$  at position  $i$ .

TVAL3 stands for "Total Variation Augmented Lagrangian Alternating Direction Algorithm", accordingly is a TV regularization algorithm which uses augmented Lagrangian and alternating direction methods, where augmented Lagrangian is a method in optimization for solving constrained problems by substitute the original constrained problem with a series unconstrained subproblems and introduce a penalty term. To solve the new subproblems the altering direction method is used [12].

As mentioned earlier in section 3.3.1 the main reason why the sequency ordered Walsh Hadamard matrix is used is to eliminate the need to store the matrix in memory during reconstruction and a promise to speed up the reconstruction. In TVAL3 there are two multiplications between matrix and a vector that dominates the computation time,

$$\Phi \mathbf{x}^k \text{ and } \Phi^\top (\Phi \mathbf{x}^k - \mathbf{y}). \quad (14)$$

The idea is to replace the multiplication with fast transforms. To explain the concept some observations and new functions need to be defined. The first observation is that the sequency ordered Walsh Hadamard matrix is a transform matrix which also can be computed with the fast Walsh Hadamard transform (fwht),

$$\mathbf{W}\mathbf{x} = \text{fwht}(\mathbf{x}), \quad (15)$$

where  $\mathbf{W}$  is a sequency ordered Walsh Hadamard matrix and  $\mathbf{x}$  is the signal vector. The wht is a generalized class of Fourier transforms which decomposes input vector into superposition of Walsh functions.

From section 3.3.1 it was briefly mention in the last paragraph that in order for the measurement matrix to fulfill RIP the columns is permuted and rows are chosen in random to create the measurement matrix from the sequency ordered Walsh Hadamard matrix, two functions is created to carry out does operations. First the permutation function  $\pi(\cdot)$ , which from a random seed permute the order of the columns in a matrix or the order of a vector. The second function  $\Pi_M(\cdot)$  chooses  $M$  row in a matrix at random and stacks them in a new matrix. Then the definition of the measurement matrix  $\Phi$  constructed from the sequency ordered Walsh Hadamard matrix  $\mathbf{W}$  leads to observation 2

$$\Phi = \pi(\Pi_M(\mathbf{W})) = \Pi_M(\pi(\mathbf{W})). \quad (16)$$

It does not matter in which order the functions i applied, it gives the same result. With matrix  $\mathbf{A}$  and vector  $\mathbf{u}$  observation 3 is formulated as,

$$\pi(\mathbf{A})\mathbf{u} = \mathbf{A}\pi(\mathbf{u}), \quad (17)$$

which shows that there is no difference between multiply a column-permuted matrix with a vector and multiply the same matrix with the vector permuted.

With all observations combined the matrix multiplication is replaced with the fwht in observation 4

$$\mathbf{y} = \Phi \mathbf{x} = \pi(\Pi_M(\mathbf{W}))\mathbf{x} = \Pi_M(\mathbf{W})\pi(\mathbf{x}) = \Pi_M(\mathbf{W}\pi(\mathbf{x})) = \Pi_M(\text{fwht}(\pi(\mathbf{x}))), \quad (18)$$

with the conclusion that the multiplication between the measurement matrix constructed using the permuted sequency ordered Walsh Hadamard matrix and the signal can be performed with the signal permuted, fast transformed using fwht and choosing rows, both permutations using the same functions  $\pi(\cdot)$  and  $\Pi_M(\cdot)$  and random seed as when the measurement matrix was created.

Using this method will reduce the overall computational complexity considerably and it will make the measurement matrix redundant in the reconstruction, only the two permutation functions  $\pi(\cdot)$  and  $\Pi_M(\cdot)$  needs to be stored. Excluding the measurement matrix in the reconstruction results in larger resolution images ( $512 \times 512$  pixels and larger) can be reconstructed. [12], [14]

### 3.5 Image capturing and processing chain

To capture an image the SPC setup is only a subsystem in the whole process from acquiring the signal to reconstructing the image. In figure 7 the whole process of capturing an image is presented with all subsystems and signal/image processing steps included.



Figure 7: Block diagram of image capturing and processing chain, from signal acquisition to final image. Each color represents different subsystems in hardware or software.

This experimental setup has no full automatic system where a button can be pressed and the system produces an image. In the setup the subsystems works completely independently and needs to be operated manually in the right order at the right time. Each color in figure 7 represents a subsystem in hardware or software. Each subsystem is described in the following subsection.

### 3.5.1 Prepare the SPC

The first step in the yellow block "Prepare the SPC" is making sure the SPC is up and running but also to point the camera at the scene and set the correct focus. The scene is located with the aid of the reference visual camera (see figure 3) with all the mirrors in the DMD directed to that camera. The focus is adjusted manually by moving the primary mirror back or forth, this procedure may introduce some error to the focus.

### 3.5.2 Sampling

The red blocks subsystem "Start sampling signal from SWIR photo diode" and "Store the raw signal" is conducted in a separate software which controls the A/D converter and thus the sampling. When the SPC is prepared the sampling of the signal is started with sampling rate such that every measurement has several sampling points thus oversampling the signal. The oversampling is needed because when the mirrors move from one pattern (measurement matrix) to the next the signal is uncertain for some time, the oversampling is also used to suppress noise from the photo diode, more on that in section 3.5.4. After the signal is sampled the obtained signal needs to be stored on the computer manually.

### 3.5.3 Streaming patterns to the DMD

The subsystem "Streaming patterns to the DMD" represented in purple in the block diagram is controlled by two different softwares, one which manipulates the pattern-signal received by the DMD and one which sends the patterns to the DMD. The patterns are sent to the DMD through a HDMI cable where the DMD is set up such that the DMD acts as a second screen to the computer. This enables to show anything on the DMD that a screen can show. The patterns are stored as a video and played back on the DMD "screen" with a media player which shows each pattern in consecutive order. This is the major bottleneck of the system where each measurement matrix needs to be

displayed one after the other depending on how fast frame rate can be achieved. The naive approach would be to display one pattern per frame which is linked to the frame rate of the DMD, lets say for example 60 frames per second (fps) then for a  $512 \times 512$  pixel large image sampled with  $M/N = 20\%$  measurement matrices gives 52428 patterns which would take

$$52428/60 = 874 \text{ seconds} = 14.5 \text{ minutes to sample which is a long exposure time for a still image with the constraint that the scene should be stationary to obtain a stationary signal.}$$

Fortunately with the software "DLP LightCrafter 4500 EVM GUI" controlling the DMD the received video signal can be manipulated before displayed onto the DMD. The software includes a function which can break down the received 24-bit color image into 1 bit planes which can be displayed in consecutive order, so for each frame received 24 patterns is encoded on that frame then the DMD software isolates each bit plane and displays them in consecutive order. This function improves the naive implementation by a factor of 24, which reduces the time to sample the image from the last example from 874 seconds to  $874/24 = 36$  seconds. This exposure time is of course not optimal for natural images outdoors but acceptably for the experimental setup.

To create the video that feeds the patterns to the DMD each pattern i.e. measurement matrix is created as presented in section 3.3.1. Then for each group of 8 unique patterns drawn from the rows of the measurement matrix are stacked in each bit plane of a 8 bit image as seen in figure 8.

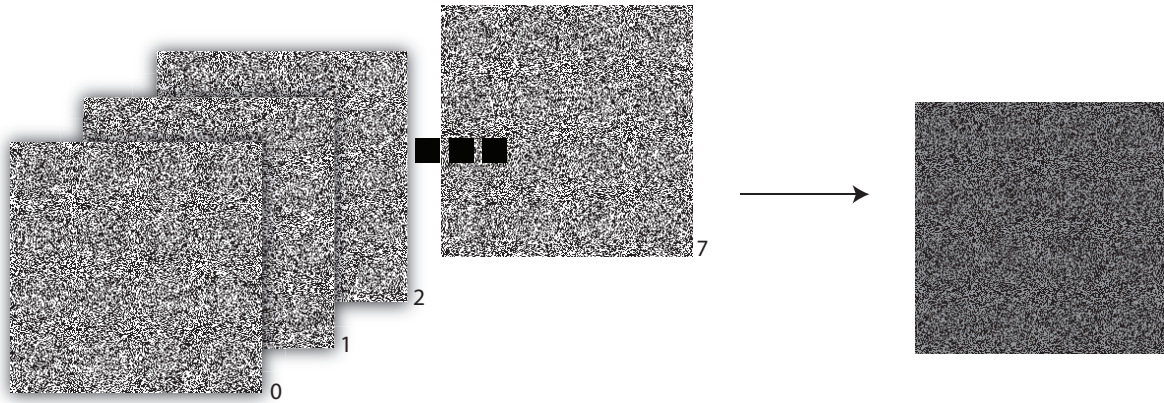


Figure 8: Stack each group of 8 measurement matrices in separate bit planes creating one 8 bit image with each matrix in one bit plane.

Then for each group of three 8 bit images a 24 bit color image is constructed as seen in figure 9.



Figure 9: Stack each group of three 8 bit plane images into one 24 bit color image. This is one frame in the video sent to the DMD.

This 24 bit color image corresponds to one frame in the video, to create the video this is done so each pattern is represented in the video.

### 3.5.4 Signal processing

When the sampled signal is stored on the computer the remaining signal/image processing and reconstruction represented by blue blocks in figure 7 is conducted in MATLAB. In this section the signal processing of the sampled signal is described.

The first step is to refine the raw over sampled signal so that each measurement matrix correspond to one measurement in signal  $\mathbf{y}$ . This is done by first find every set of indices corresponds to every measurement matrix, as seen in figure 10 where the signal indices which corresponds to one measurement matrix is isolated by the purple lines.

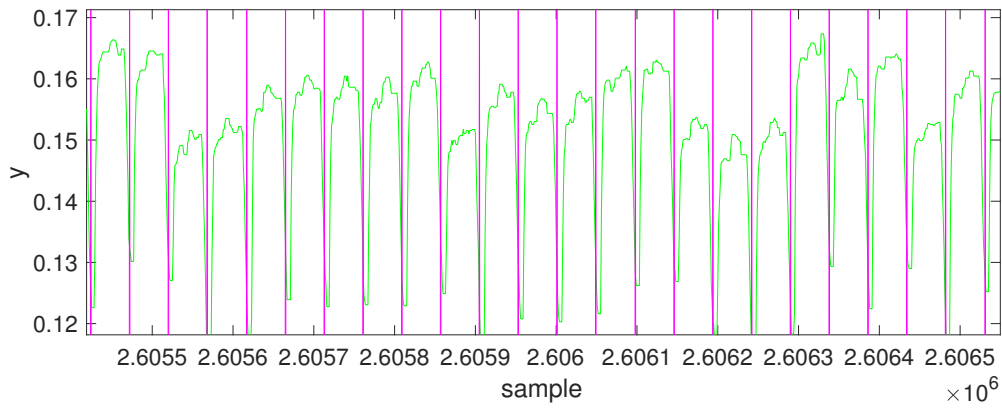


Figure 10: —

The next step is to determine one value for each measurement. This is done in two steps the first is to omit values which corresponds to the DMD changing pattern seen in figure 10 where the purple line divides the measurements the DMD is changing pattern which gives an uncertain signal. With

the omitted parts of the signal corresponding to one measurement the mean is calculated and set to the value for each measurement, as seen in figure 11.

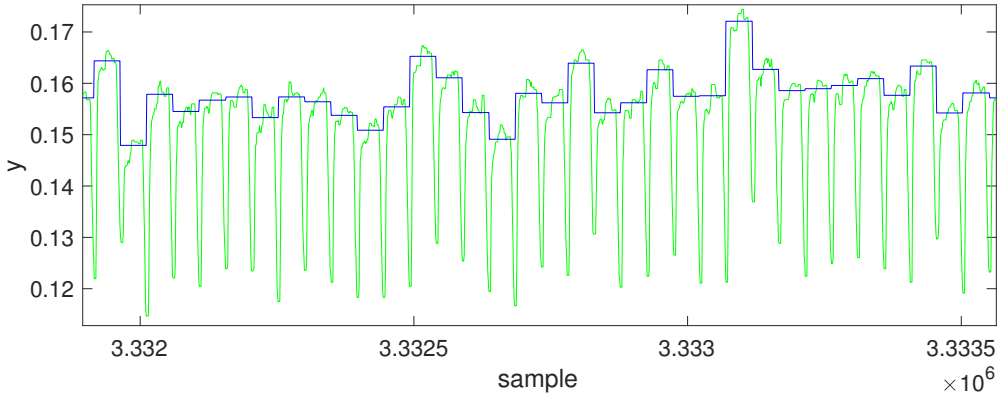


Figure 11: —

### 3.5.5 Dynamics in scene

So far the measurement vector  $\mathbf{y}$  has been determined, in the ideal case even with added noise the measured signal should be stationary because the image is assumed to be constant with half the pixels measured at random uniformed spread across the image. Each pixel in the image has the same value in each measurement with some noise added which is divided by all pixels being measured i.e. half the pixels which does not have a significant impact of the reconstructed image. But when capturing images outdoors with natural light in addition with long exposure time as described in section 3.5.3 it is not certain that the image (or every pixel) is constant over the exposure time which will reduce reconstruction performance because of the ambiguity of each pixel. The potential dynamics in a scene can be divided into two categories: luminance change and object movement. In this subsection the luminance change problem is modeled with corresponding algorithm to suppress the impact on the reconstructed image. The object movement problem will not be modeled, instead be avoided when capturing the signal by making sure the scene is as static as possible.

In natural outdoor images it can be assumed the the primary source of light comes from the sun, but even on a clear day the light intensity from the sun is not constant. If the scene is assumed to be completely stationary even the slightest intensity change will be added for all pixels being measured changing the mean intensity of the measured signal  $\mathbf{y}$  which should be stationary. With the assumption that the image is constant and the luminance change uniformly adds the same intensity to each pixel per measurement the problem can be modeled.

Start of with the original theorem and disregard the noise,

$$\mathbf{y} = \Phi\mathbf{x}, \quad (19)$$

the image  $\mathbf{x}$  can not longer be considered constant for all measurements, the luminance change will change image  $\mathbf{x}$  for every measurement matrix  $\Phi_i$  depending on the uniform luminance change. This can be described for one measurement as,

$$y_i = \Phi_i \mathbf{x}_i = \Phi_i(\mathbf{x} + \mathbf{l}_i) = \Phi_i \mathbf{x} + \Phi_i \mathbf{l}_i, \quad (20)$$

where  $\mathbf{l}_i$  uniform adds the same intensity over the whole image  $\mathbf{x}$  for measurement  $i$ . It is known from before that the measurement matrix  $\Phi_i$  contains 50% zeros and ones which gives,

$$y_i = \Phi_i \mathbf{x} + \Phi_i \mathbf{l}_i = \Phi_i \mathbf{x} + \frac{N}{2} c_i, \quad (21)$$

where  $c_i$  is the uniform intensity change coefficient for measurement  $i$ . This function can be generalized for all measurements,

$$\mathbf{y} = \Phi \mathbf{x} + \frac{N}{2} \mathbf{c} = \Phi \mathbf{x} + \mathbf{c}, \quad (22)$$

where  $\mathbf{c}$  is the intensity change vector.

The goal is now to remove the intensity change vector from signal  $\mathbf{y}$ . Using the knowledge that the signal  $\mathbf{y}$  should be stationary and assumes that the rate of change in intensity has a much lower frequency than the intensity change between individual measurement matrices, then  $\mathbf{c}$  can be approximated by the moving average and simply removed from signal  $\mathbf{y}$ . The moving average is calculated at each data point in the signal vector  $\mathbf{y}$  by calculating the average of  $k$  points centered around the data point.

### 3.5.6 Reconstruction

Reconstruction is performed using the TVAL3 algorithm described in section 3.4.1. The algorithm takes in measurement matrix  $\Phi$ , signal  $\mathbf{y}$  and algorithm settings as arguments and outputs the reconstructed image. The setting used throughout all experiments is:

- $opts.mu = 2024$
- $opts.beta = 64$
- $opts.maxcnt = 10$
- $opts.maxit = 1000$
- $opts.tol\_inn = 10^{-5}$
- $opts.tol = 10^{-10}$
- $opts.mu0 = 2^4$
- $opts.beta0 = 2^0$
- $opts.nonneg = \text{true}$
- $opts.isreal = \text{true}$

Which solves for a real non negative solution described in section 3.4.1.

### 3.5.7 Image processing

From the reconstructed image some light image processing is done. There are only two operations applied to the reconstructed image and the reason why is that the images presented in the evaluation should represent what can be expected from the system. Furthermore often image processing is applied on special problems or artifacts in the images and it is not desired to cover up if there exist such problems. Therefore the two operations used is median filter and adjusting the intensity for higher contrast.

The reconstructed image has a high dynamic range and if only a small set of neighboring pixels is reconstructed with a high intensity peak which not correlates to the rest of the image these pixels will drop the contrast in the rest of the image, to remove these peaks the median filter is used. The

median filter will also remove "salt and pepper" noise while edges are preserved. The built in MATLAB function *medfilt2* will be used.

The second operation is an intensity transform to maximize the contrast in the image, the built in MATLAB function *imadjust* will be used.

### 3.6 Evaluation: Image quality assessment

The evaluation will be divided in to two categories: reconstructed images from synthetic data and images reconstructed from data acquired by the SPC.

The evaluation on synthetic data is focused on evaluating the performance of the measurement matrix and reconstruction algorithm. Evaluating synthetic data gives two possibilities that can not be achieved with images reconstructed using the SPC which is that there is a reference image which the resulting image can be compared to.

Reconstructed image from synthetic data is acquired by creating a signal  $\mathbf{y}_{M \times 1}$  taking the inner product of  $\mathbf{y} = \Phi\mathbf{x} + \epsilon$  where,  $\mathbf{x}$  is the synthetic image reshaped to a vector,  $\Phi$  is the measurement matrix with the desired amount of measurements  $M$  and synthetic noise  $\epsilon$  which can be regulated to simulate different conditions, then using the reconstruction algorithm on the signal  $\mathbf{y}$  to obtain the reconstructed image  $\hat{\mathbf{x}}$ . Because the measurement matrix and reconstruction algorithm is independent of the SPC hardware the subsystem can be evaluated independently. Two advantages of evaluation the sensing and reconstruction independently of the SPC is that parameters such as number of measurements and noise can be regulated easy and the second advantage is that a reference image is available for comparison.

With a reference image available two image quality assessments are performed on the result from the simulation: Peak signal-to-noise ratio (PSNR) and SSIM. PSNR is defined as

$$\text{PSNR}[f(x, y), g(x, y)] = 10 \log_{10} \frac{E^2}{\text{MSE}[f(x, y), g(x, y)]} \quad (23)$$

where,  $f(x, y)$  and  $g(x, y)$  is intensity in pixel  $(x, y)$  and MSE is the mean square error between the images defined as

$$\text{MSE}[f(x, y), g(x, y)] = \frac{1}{mn} \sum_{x=0}^{y-1} \sum_{n=0}^{n-1} [f(x, y) - g(x, y)]^2. \quad (24)$$

Large syntetic test of SWIR images, Whar result can be expected

Synthetic test of the methods presented in section 3.5.4 will be conducted to measure the performance and validity.

Number of measurements needed to get a good image

Homography test

Brisque

MTF which measures Edge response

### 3.7 Method criticism

- No Reference Image Quality Assessment is not designed for SWIR images or SPC:s characteristics noise therefore the results may not reflect how the QA would answer to visual wavelength cameras.

## 4 Evaluation

This section is structured as, for each experiment and setup a detailed explanation and motivation on how and why the experiment is needed followed by the results of that experiment. The experiments are motivated by gathering as much information and results as possible to answer the research questions. The first subsection 4.1 will present the results from experiments with synthetic data where a reference image is available. The second subsection 4.2 will present the result from images reconstructed from the SPC. No perfect reference image is available in those experiments therefore the images will be evaluated against near optimal image, no reference QA and against a state of the art SWIR camera.

### 4.1 Simulated results

In this section the results produced was simulated by using the reconstructing algorithm and measurement matrix described in section 3.4.1 and 3.3.1 on high quality images captured with a state of the art SWIR camera. The images captured by the SWIR camera acts as a ideal reference to the reconstructed images. By simulating the result from "ideal" images the reconstruction process gets a benchmark independent of the SPC.

#### 4.1.1 Reconstruction performance using reference image

In these simulation 21 images captured with a state of the art SWIR camera was reconstructed. The performance of the reconstruction was calculated using PSNR and SSIM for different degree of noise and sub sampling ratios.

To reconstruct the images first the measurement vector was created by calculating the inner product between the measurement matrix  $\Phi$  and SWIR image  $\mathbf{x}$ ,

$$\mathbf{y}_{IDEAL} = \Phi \mathbf{x}, \quad (25)$$

where  $\mathbf{y}_{IDEAL}$  is an ideal measurement vector given  $\Phi$  and  $\mathbf{x}$ . In the next step white Gaussian noise was added to the normalized measurement signal. The added noise represent a simple model of the noise perturbing the signal in the SPC.

$$\mathbf{y}_R = \mathbf{y}_{IDEAL\_NORMALIZED} + \epsilon, \quad (26)$$

where  $\mathbf{y}_R$  is the measurement vector used when reconstructing the image and the white Gaussian noise  $\epsilon$  added was scaled with the standard deviation  $\sigma$  between  $0 - 0.2$ .

To create the graphs in figure 13 and 14 this procedure was applied to all 21 images for sub sampling ratio 5% to 30% and added noise with standard deviation between  $0 - 0.2$ . The standard deviation is not increased above 0.2 because the reconstruction fails at that point. In figure 12 a sample of reconstructed image from one of the SWIR images is presented with different amount of noise and sub sampling ratios.

Describe  
how the  
graphs was  
created



(a) Reference image

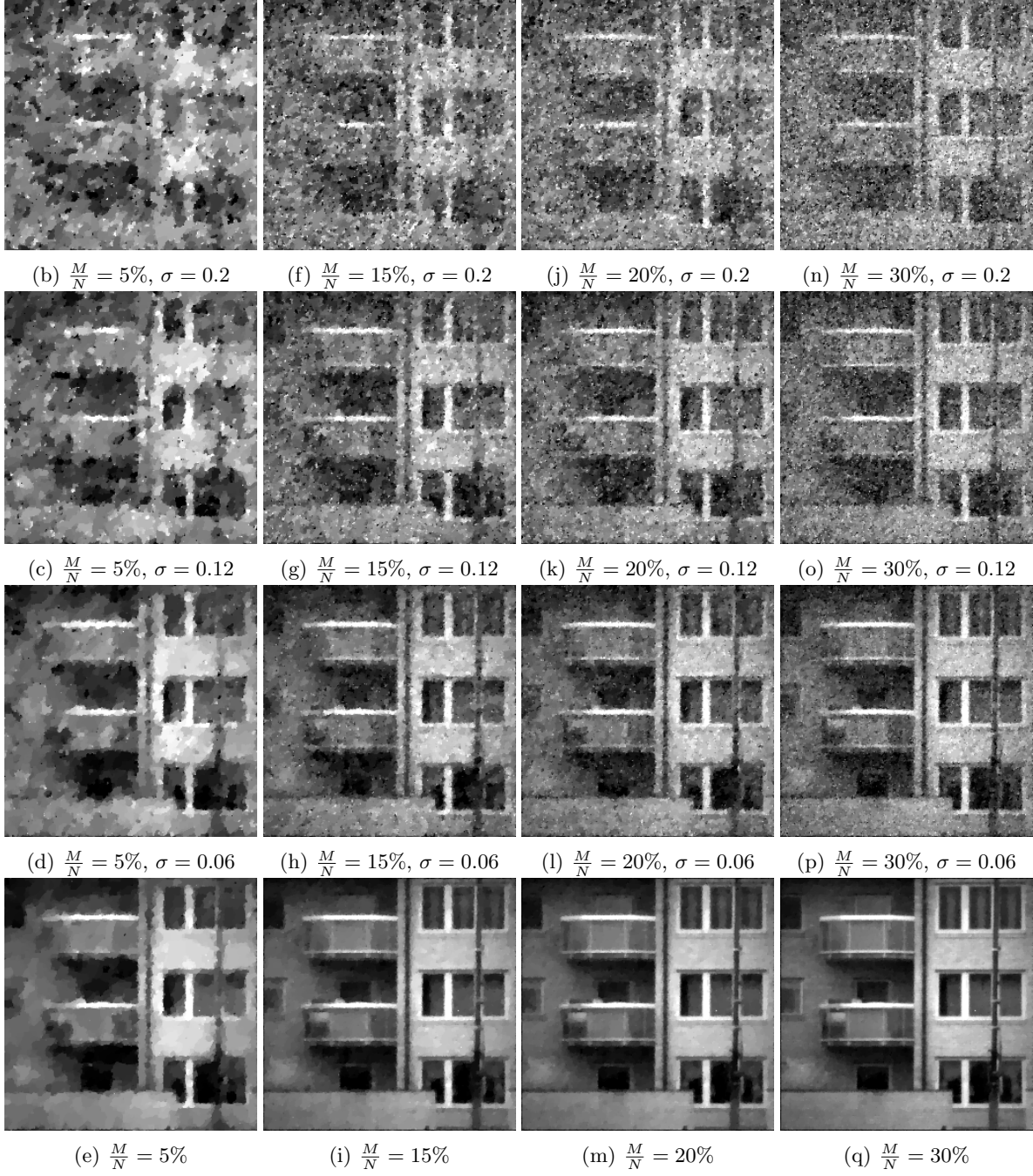


Figure 12: Example of reconstructed images with added noise at different sub sampling ratios.

As seen in figure 12 the reconstructed image quality increases with more measurements and lower noise levels. This observation is confirmed in the graphs i figure 13 and 14 where PSNR and SSIM respectively has been calculated for all 21 reconstructed images and interpolated.

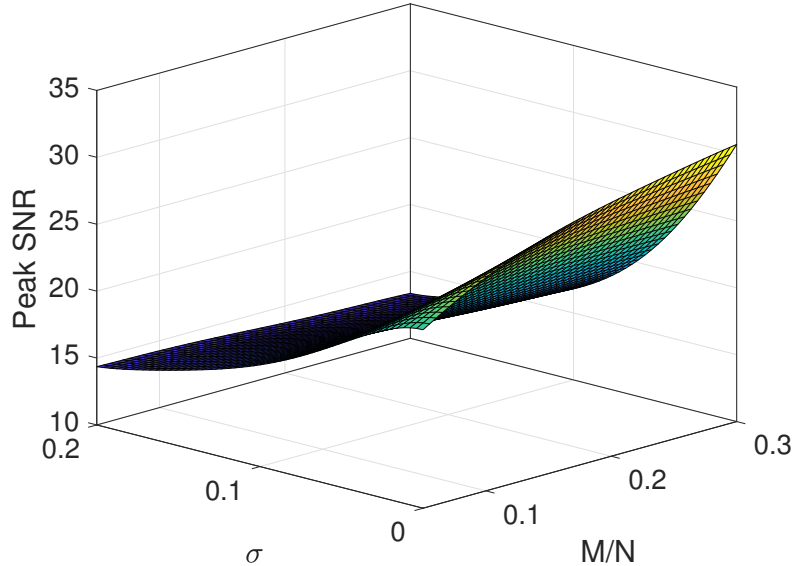


Figure 13: Peak SNR result depending on number of measurements and simulated noise level.

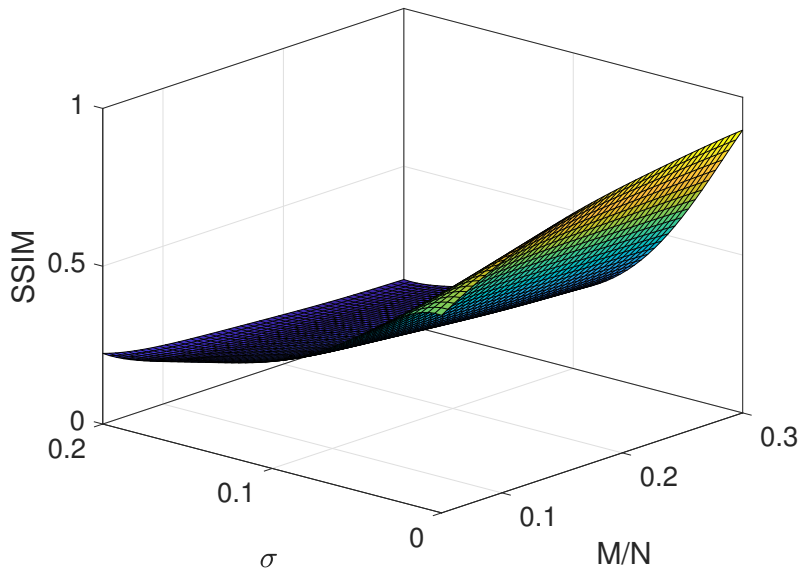


Figure 14: SSIM result depending on number of measurements and simulated noise level.

A second observation is that, when the noise increases the reconstructed image quality is not improved at the same rate as the noiseless case when increasing the sub sampling ratio, meaning that a bad signal can not be salvaged by more measurements.

#### 4.1.2 Reconstruction performance using no reference quality assessment

In this sub section the same reconstructed image set from section 4.1.1 is used to calculate the no reference image quality with the BRISQUE algorithm. This is the same algorithm which will be used to evaluate the results from the SPC therefore this experiments will yield a benchmark on how good results that can be obtained given the measurement matrix and reconstruction algorithm.

The results displayed in the graph in figure 15 shows the same trend as the results from the previous section, less noise and more samples yields better performance in the reconstruction. The figure also contain the mean results from the original SWIR images as the flat blue surface, which has scored a far superior score then the reconstructed images.

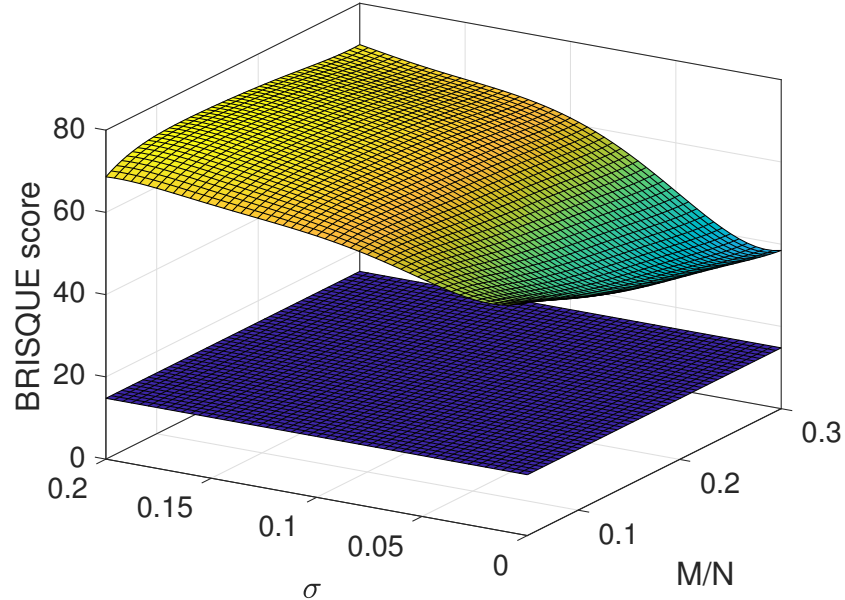


Figure 15: BRISQUE result depending on number of measurements and simulated noise level. Lower surface is reference image score.

In figure 16 the result has been flatten to a 2D graph with fewer selected data points for clarity. Even in the noiseless case the score will not be better then approximately 40 for the reconstructed images while the SWIR images has a mean value of 15. The conclusion from this result is that, with the current measurement matrix and reconstruction method around 40 in BRISQUE score is what to expect as optimum given that the SPC will induce noise to the signal.

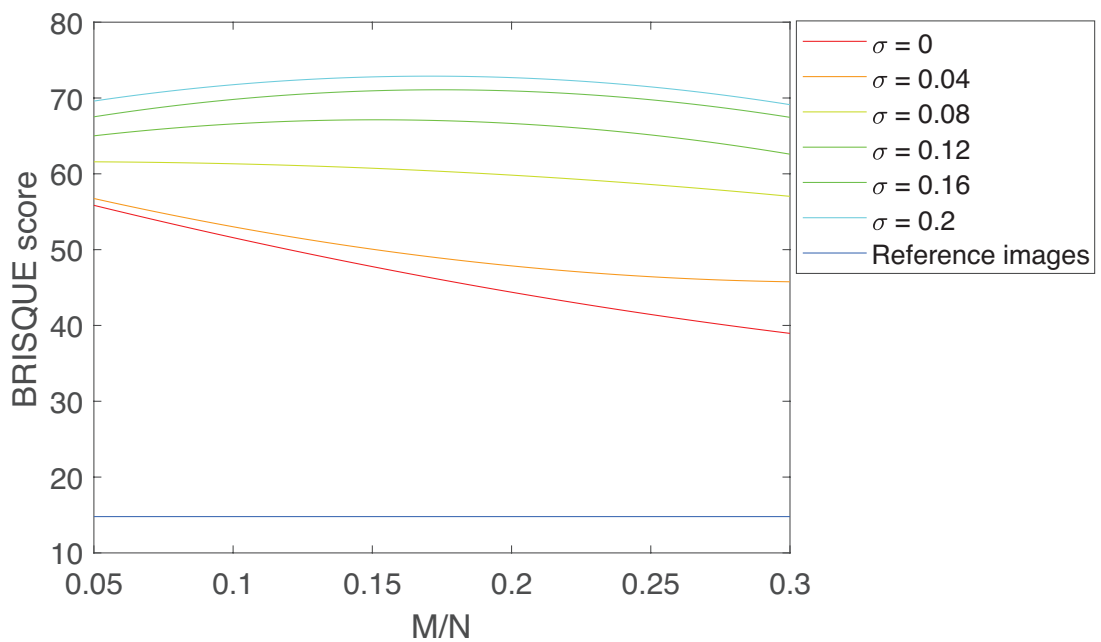


Figure 16: BRISQUE result depending on number of measurements for different simulated noise levels.

#### 4.1.3 Dynamics in scene

In the current experimental SPC setup the exposure time is between 10 to 50 seconds which increases the chance of dynamics in the scene. Dynamics in the scene will reduce the reconstruction performance because the signal is assumed to be constant. By simulating dynamics in a controlled environment the measured signal characteristics for different cases can be identified. Dynamics in the scene can roughly be roughly divided into two separate categories, luminance change and movement. In this section global luminance change and two kinds of motion be simulated. The goal is to interpret how the signal change and if it can be suppressed for better reconstruction.

In the first scenario a object is placed in an image but for each measurement the location of the object will be moved in a bounded area of the image. This model represents a scene where the background is static but a person is standing in the same area but moves around.

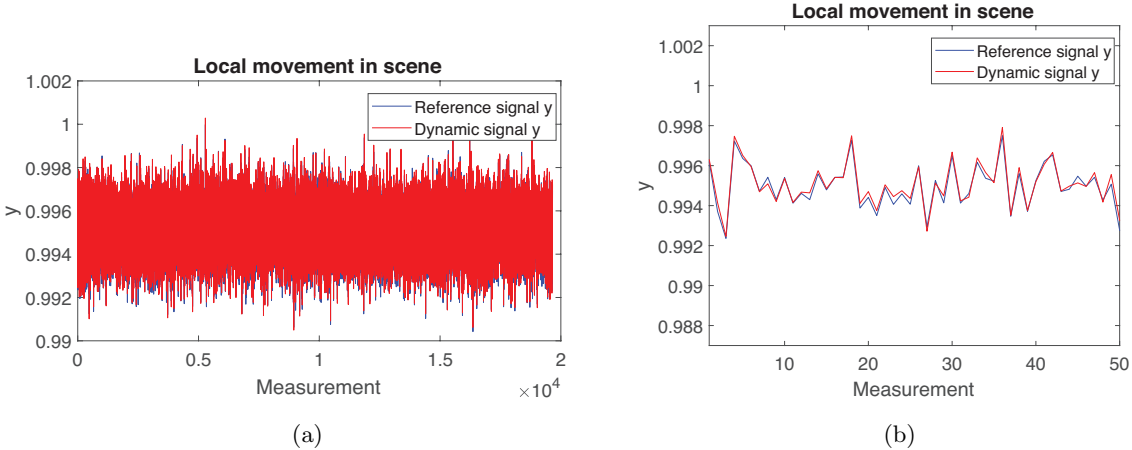


Figure 17: (a) Perturbed signal from local movement on top of reference signal. (b) Zoomed in view of some samples from figure (a).

As seen in figure 17a there is no obvious difference between the non perturbed reference signal and the distorted signal. In figure 17b where some of the samples is displayed no large difference can be seen either. It can be interpreted as added noise to the signal and it is barely detectable even if the signal is known.

The reconstructed images from the reference signal and the perturbed signal is displayed in figure 18b and 18c respectively. The difference between the reconstructed images is visible to the naked eye, not only does the object moving around get blurry and noisy but the whole image globally.

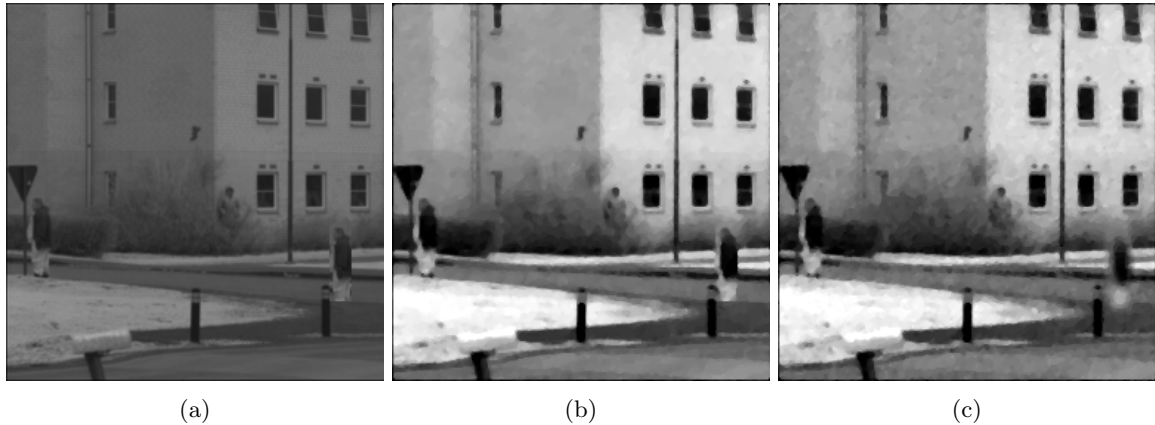


Figure 18: The results of local movement on a reconstructed image, sub sampled at 30%. (a) Original reference image. (b) Reference image reconstructed from the original image without movement. (c) Reconstructed image from a scene with local movement.

In table 2 the results from calculating PSNR and SSIM between the reconstructed images is presented. It can be observed that the image has been effected to some degree by the movement.

Peak SNR	SSIM
29	91

Table 2: Effects comparing non perturbed reconstructed image against reconstructed image with local movement

The conclusion of this test implies that local movement in a scene will cause noise in the image globally and especially locally where the movement occurred. It also implies that local movement is very hard to detect in the signal even if a reference signal is available.

The second scenario is an object passing through, moves out or moves to an other place in the scene far from the original place. The problem is modeled with a static background then as the simulated measurement is acquired the object will cross the scene, like a car, human or animal might do when using the SPC. The object will cross the scene in 1000 measurements of approximately 19000 which corresponds to approximately 0.7 seconds when sampling measurements with the SPC in its current setup.

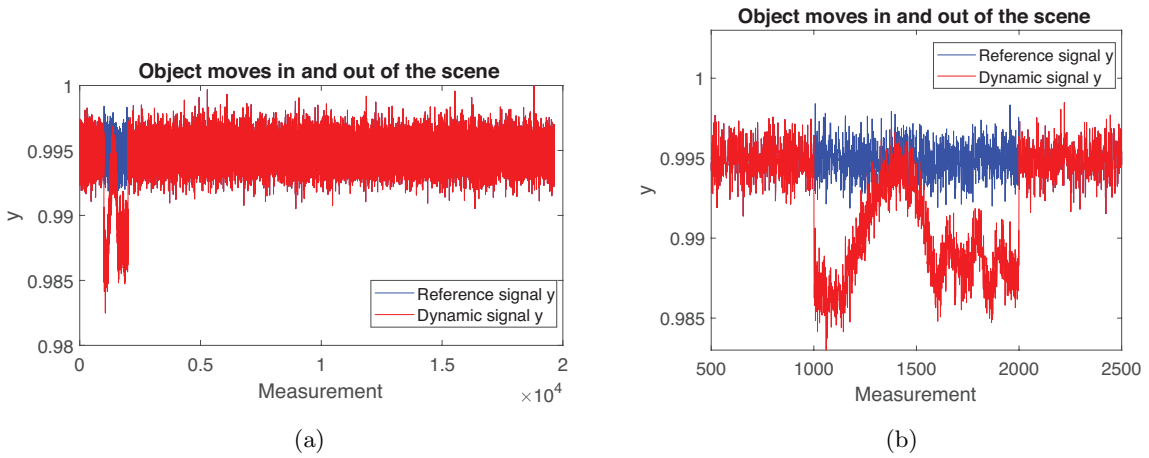


Figure 19: (a) Perturbed signal from large movement on top of reference signal. (b) Zoomed in view of some samples from figure (a).

As seen in figure 19 the exact moment the object enters the scene the signal changes. This is because a completely new structure has entered the scene and therefore changing the DC level. It can also be noted that the object passed something which has approximately the same intensity as the background and therefore the DC signal almost comes back up to its original state for a brief moment.

In figure 20 the effect of the moving object can be seen in the reconstructed image which has gained a lot of global noise. Note that the object passing through can not be seen because there is more measurements with the background and the object moving creating uncertainty in the whole image.

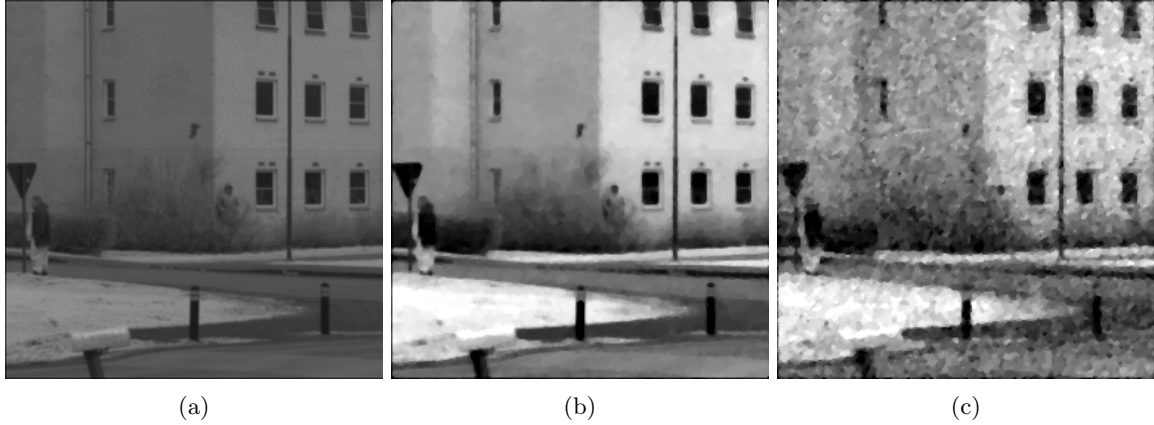


Figure 20: The results of large movement on a reconstructed image, sub sampled at 30%. (a) Original reference image. (b) Reference image reconstructed from the original image without movement. (c) Reconstructed image from a scene with object passing through.

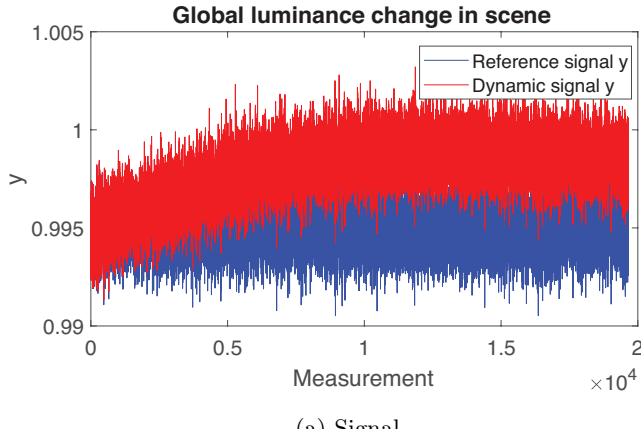
In table 3 the results from calculating PSNR and SSIM between the reconstructed images is presented. It can be observed that the image has been effected heavily by the movement.

Peak SNR	SNR	SSIM
23	18	58

Table 3: Effects comparing non perturbed reconstructed image against reconstructed image with local movement

Obviously in this context the samples with movement is very easy to spot and the easiest fix would be to just remove those measurements, reconstructing an image with fewer measurements. The resulting image would not be as good as the image in figure 20b but it would not contain the noise present in figure 20c.

The third scenario is luminance change in the scene which is caused by inconsistency of light intensity from the source. Outdoors this means that the light intensity from the sun will vary over time, the most obvious being clouds occluding the sun but even change in air density can change the intensity. This scenario is modeled by adding or subtracting the global intensity in the image over the measurements.



(a) Signal.

As seen in figure 21a the DC level of the signal will slowly change but the structure of the signal stay the same. In figure 22 the reconstructed images from the perturbed signal and the reference signal is displayed. The reconstructed image from the dynamic signal has gained a lot of global noise even though the structure in the image has not been changed over the measurements.

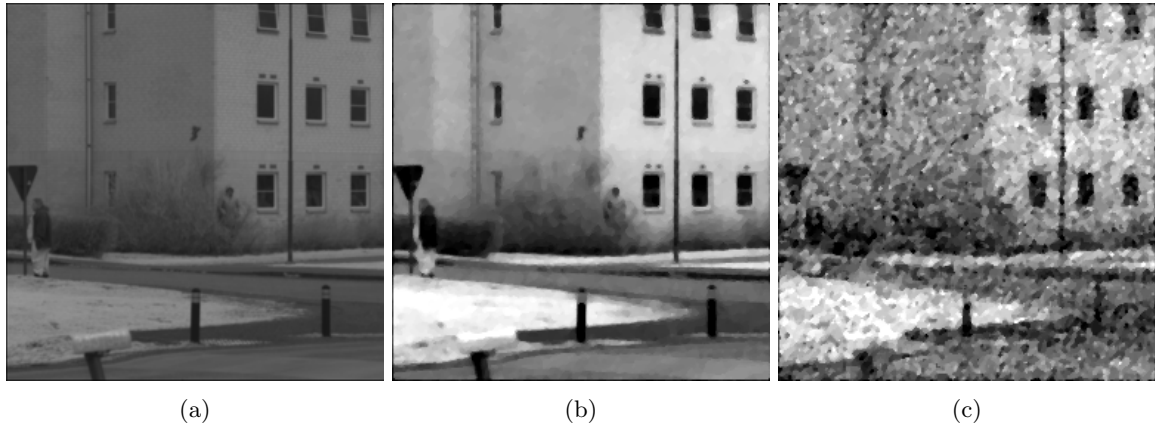


Figure 22: The result of global light intensity change on a reconstructed image sub sampled at 30%  
 (a) Original reference image. (b) Reference image reconstructed from the original image without light intensity change. (c) Reconstructed image from a scene with global light intensity change over the measurements.

In section 3.5.5 a model of this problem was proposed with a algorithm to suppress the impact of global luminance change. The algorithm is applied to this experiment to evaluate its performance. The moving average subtraction method is applied and in figure 23a the resulting signal is plotted over the dynamic signal, the improved signal is stationary again. In figure 23b and 23c where the processed signal is plotted over the reference signal it can be seen that the processed signal has gained its original structure and almost fit exactly to the original.

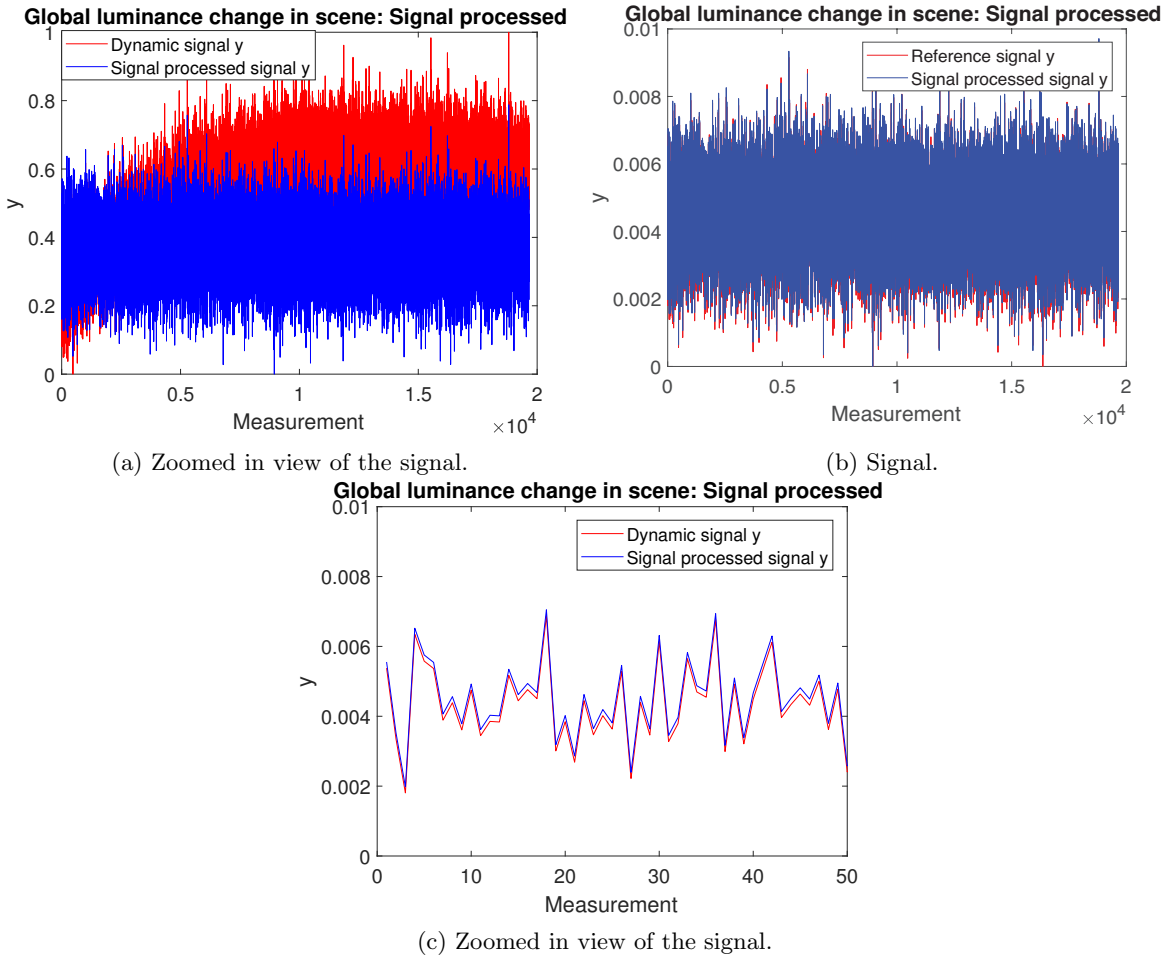


Figure 23: Global movement, acquired signal

In figure 24 the processed signals reconstructed image is displayed between the reference and perturbed signals reconstructed images. The signal processing improve the reconstruction significantly, the image has gained some noise compared to the reference image but over all there is not much difference between them.

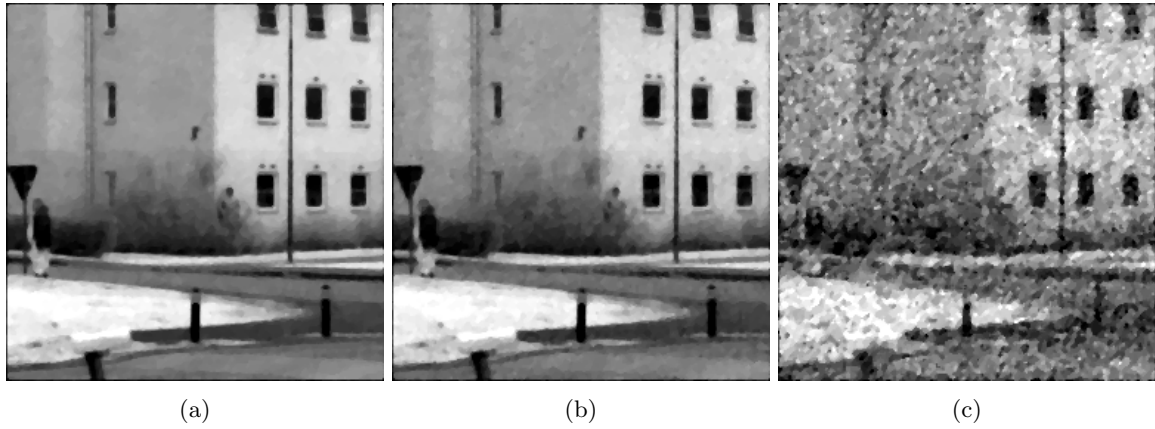


Figure 24: The result of processed signal perturbed by light intensity change on a reconstructed image sub sampled at 30% (a) Reference image reconstructed from the non perturbed signal without light intensity change. (b) Reconstructed image from a scene with global light intensity change over the measurements signal processed. (c)Reconstructed image from a scene with global light intensity change over the measurements.

In table 4 the results from calculating PSNR and SSIM between the reconstructed images is presented. The effect on the perturbed signal is worse than scenes containing movement meaning that this problem can cause very bad reconstruction performance for natural images, but the algorithm handle the problem well which can be seen in PSNR, SSIM and the reconstructed image.

	Peak SNR	SSIM
Perturbed signal	19	38
Mean subtracted signal	33	93

Table 4: Effects comparing non perturbed reconstructed image against global luminance change perturbed reconstructed image and mean subtracted signal reconstructed image.

## 4.2 SPC evaluation

The evaluation section is now shifted to examine the images produced by the SPC. The images will be analyzed using the using a range of methods to examine the performance of the SPC. In this section the BRISQUE algorithm will be used again where connections to the previous result is drawn, a reconstructed image will be compared to an ideal image using homography, a set of images is presented reconstructed at different subsampling ratios, a edge response analysis i performed and the correlation between reconstruction performance and noise is conducted.

### 4.2.1 Image quality using no reference quality assessment

In this section the blind quality assessment tool BRISQUE will be used to score the reconstructed images from the SPC. The same algorithm was used on the simulated data where a benchmark was set as a theoretical limit to the reconstructed images.

Each image is evaluated at subsampling rate from 5% to 30% where the result is presented in figure 25.

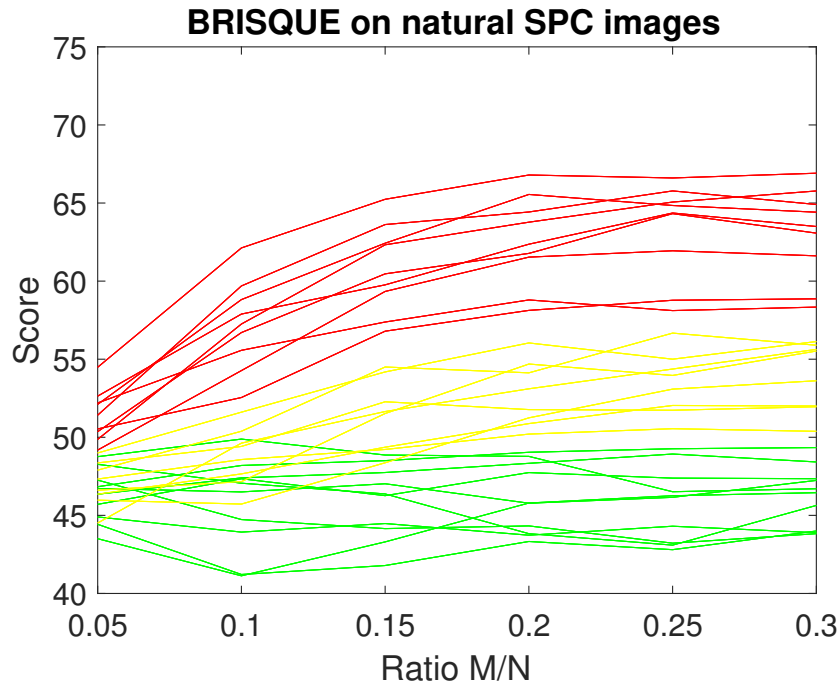


Figure 25: BRISQUE score for images reconstructed from the SPC with subsampling ratios from 5% to 30%. Each line represent one image and is classified with different colors representing start score at smallest subsampling ratio and general trend when subsampling ratio is increased.

As seen in figure 25 each image has been plotted separately, this is because the high variance in the scores and the distinct different trends in the score. Furthermore the images has been classified into three different classes depending on the initial score at 5% subsampling and the trend when increasing the subsampling ratio. The classes has been color coded where:

- Red means bad score from the first subsampling ratio and a trend line where the score gets worse with more samples.
- Yellow represent good initial score but the trend line indicates worse image quality when subsampling ratio is increased.

- Green represent both good initial score and better or stationary score when subsampling ratio is increased.

When studying the BRISQUE score plot in figure 25 from the SPC and comparing to the plot of BRISQUE scores from simulated images in figure 16 some similarities can be found. The first one is that, the best scores from the SPC has the same score as the simulated images with small or no noise added, which means that the SPC can compare to the benchmark set by the simulated images and thus gives theoretical optimal reconstruction given the measurement matrix and reconstruction algorithm. The second similarity is the trend of the "bad" images which has approximately the same score and trend as the simulated images with larger noise added to the sampled signal. In the last part of this subsection the reconstructed images will first be presented an analyzed followed by a noise analysis to conclude if there is a correlation between noise level and BRISQUE score.

In figure 26 to 28 a sample of reconstructed images are presented from each class with subsampling ratio 30%.

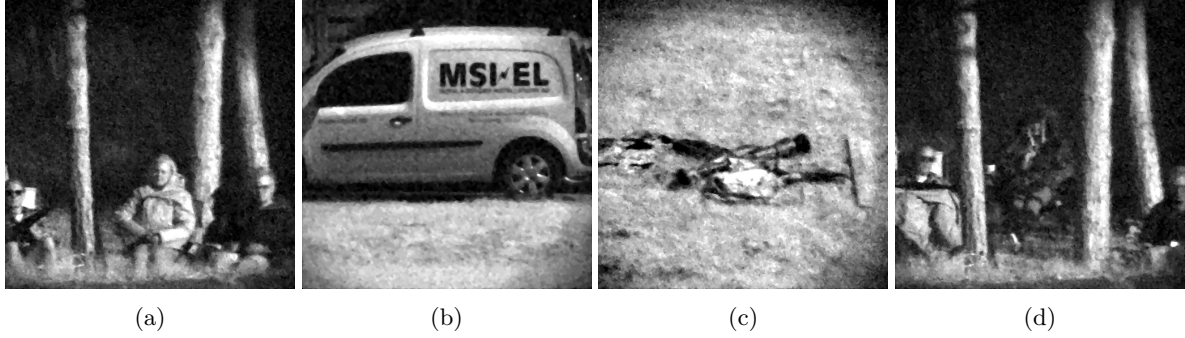


Figure 26: Sample of "good" images corresponding to the green lines in figure 25. (a) and (d) People sitting in the edge of a forest. (b) Stationary car. (c) Camouflage jackets and a AT-4 anti-tank weapon on the ground.

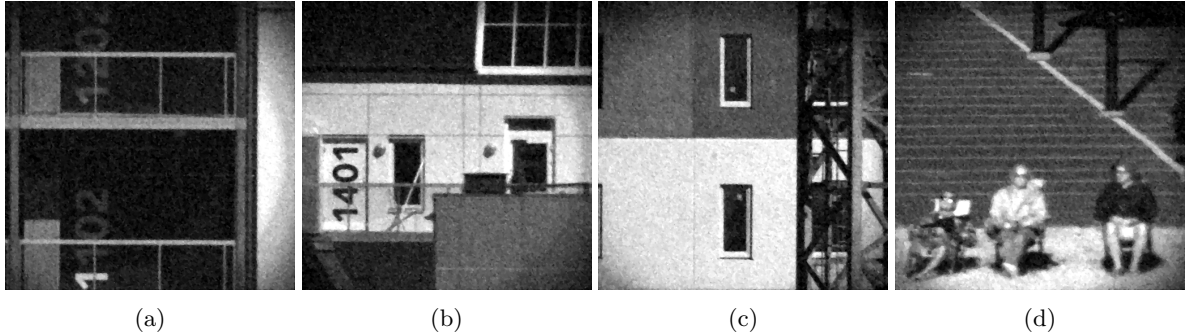


Figure 27: Sample of "medium good" images corresponding to the yellow lines in figure 25. (a) People sitting next to a parking lot. (b) - (d) House facades.

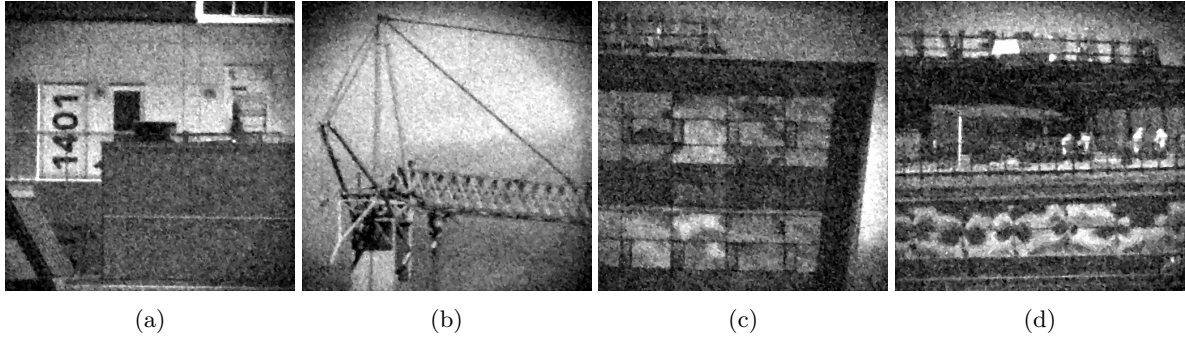


Figure 28: Sample of "bad" images corresponding to the red lines in figure 25. (a) House facade. (b) Crane. (c) Mjärdevi Center facade (d) Mjärdevi Center balcony with people having a break.

Lets analyze the images in figure 26 to 28 in order to figure out why the BRISQUE score have such high variance and characteristics when increasing the subsampling ratio. The difference between "good" and "half good" images are very subtle, the intensity and visible noise level is a bit more favorable in the "good" images, but as stated in section 3.6 the naturalness of the images differ where the "good" images contains more natural shapes and objects. Between the "good"/"half good" and "bad" images there is a more noticeable difference, the images in the "bad" set has more distinct noise and lower over all intensity which most certainly effect the BRISQUE score. Furthermore some of the "bad" image set had movement when sampled which will definitely increase global noise in the images as concluded in section 3.5.5.

When the images was sampled a correlation between the mean signal strength and reconstruction performance was noticed, this is due to the constant background noise from the SWIR photo diode. In figure 29 the mean sampled signal strength was plotted against SNR and signal variance calculated from normalizing the sample signal and background noise. The variance was calculated in the same way as the simulated signals in section 4.1. Each signal has the same corresponding color code from the BRISQUE plot in figure 25.

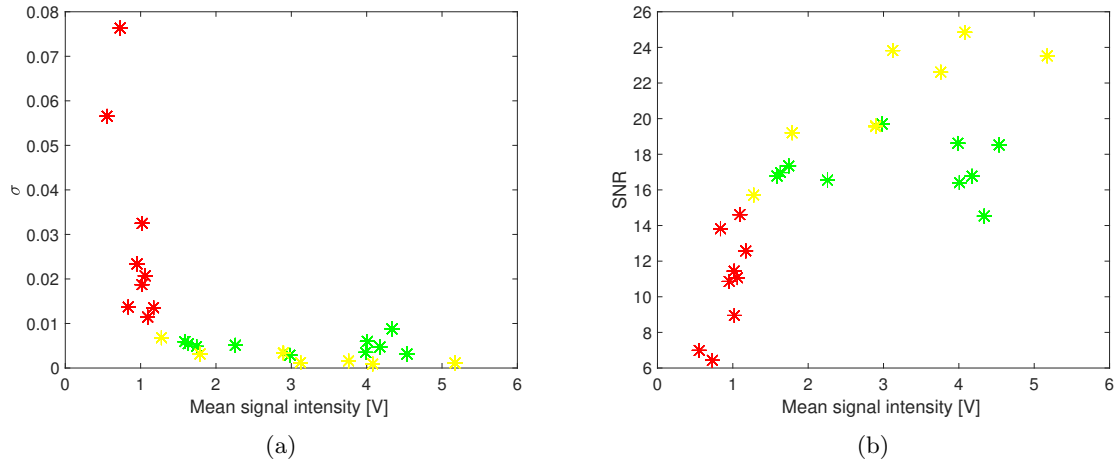


Figure 29: Mean sampled signal intensity compared to normalized signal and background noise where each signal has the same corresponding color code from the BRISQUE plot in figure 25. (a) Signal intensity against normalized variance from background noise. (b) Signal intensity against SNR from normalized signal and background noise.

From the two plots in figure 29 there are some conclusions that can be made:

- From both plots in figure 29 there is a quite distinct threshold where the signals intensity overcomes the noise level to reconstructed "good" images around 1.2 volt. None of the "good"/"half good" images is below this signal intensity but is mixed over the threshold.
- In the plots there is only two signals with higher variance than 0.04 which is the threshold where the the simulated images started to get both worse initial BRISQUE score and worse trend when increasing the subsampling ratio in figure 16. This implies that there must be at least one additional factor in play to reduce the image quality in the "bad" set.
- 
- We can see that some red images almoast has the same SNR and mean signal intesity as yellow and greeen images but yelds a worse BRISQUE score anyway.

#### 4.2.2 Number of measurements



(a) m15

(b) m10

(c) m10



Figure 31: Images reconstructed using  $M/N = 5\%$  to  $30\%$  measurements from top down.

#### 4.2.3 Soft chessboard

**Todo:** Skapa rekonstruerade bilder från homographin och jämför de rekonstruerade med referensbilden

This evaluation is designed to confirm that the images reconstructed by the SPC follows the same characteristics as the reconstruction of the synthetic data.

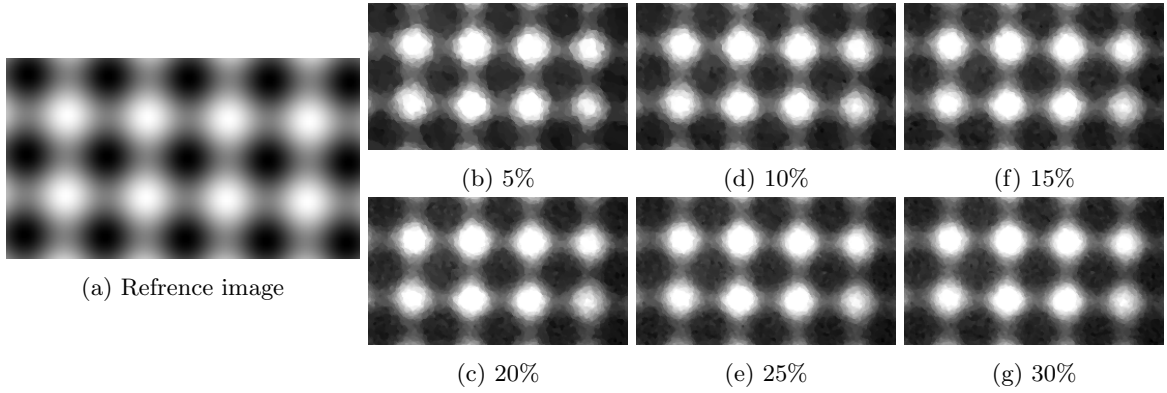


Figure 32: The reconstructed images with different number of measurements and the reference image transformed to fit the SPC images using homography.

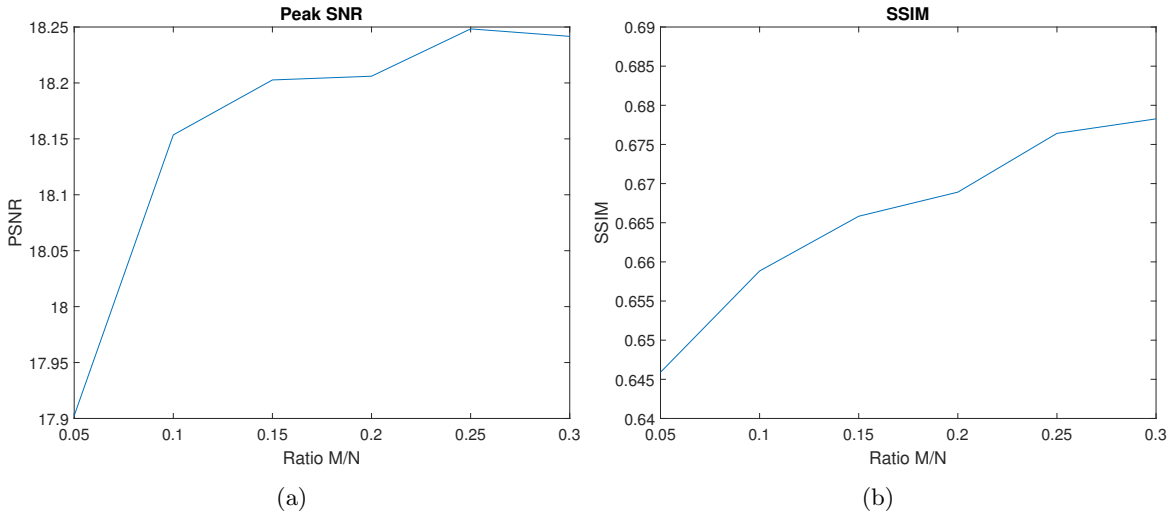


Figure 33: Signal quality of SPC images compared to reference image. (a) Peak SNR for reconstructed images against reference image. (b) SSIM score for reconstructed images against reference image.

#### 4.2.4 Modulation Transfer Function

The MTF is used to comparing the sharpness of cameras and lenses.

The MTF from the SPC is compared to a state of the art SWIR camera. Two scenes was captured by the SPC and a conventional SWIR camera containing printed sheath of paper with simple tilted shapes on them, see figure 34.

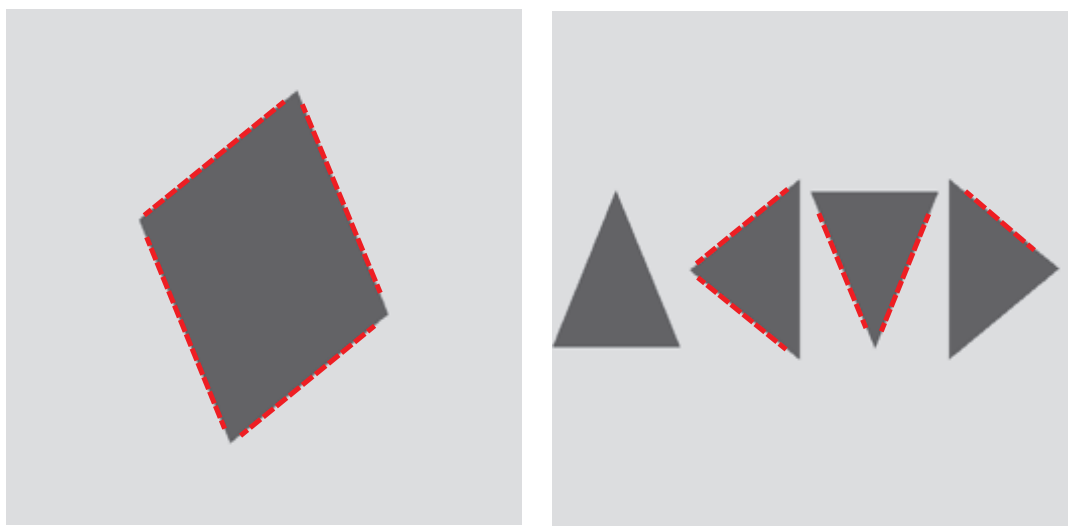


Figure 34: Printed targets with markings where the MTF measurements was performed

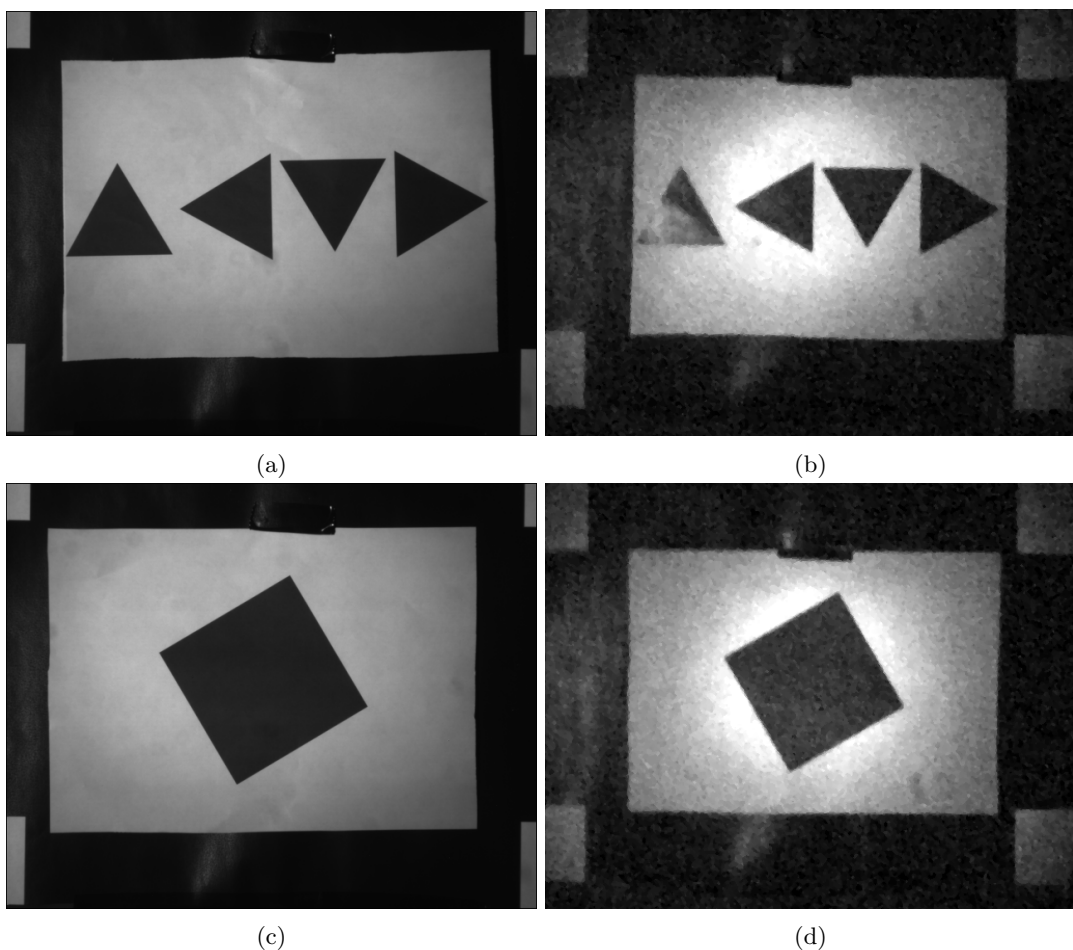


Figure 35: SPC and state of the art SWIR camera output images.

In the resulting images MTF measurements was performed on the specified edges to gather a mean and standard deviation for each camera. For the SPC, images reconstructed from 5% to 30% was tested in order to see if the number of measurements effected the MTF result. In figure 35 the images from the SWIR camera and SPC are presented.

Light source 135W from 2m. Image on the board

The edge response is measured in the distance (pixels) required for the edge to rise from 10% to 90%. In figure 36 the result from the experiment is presented.

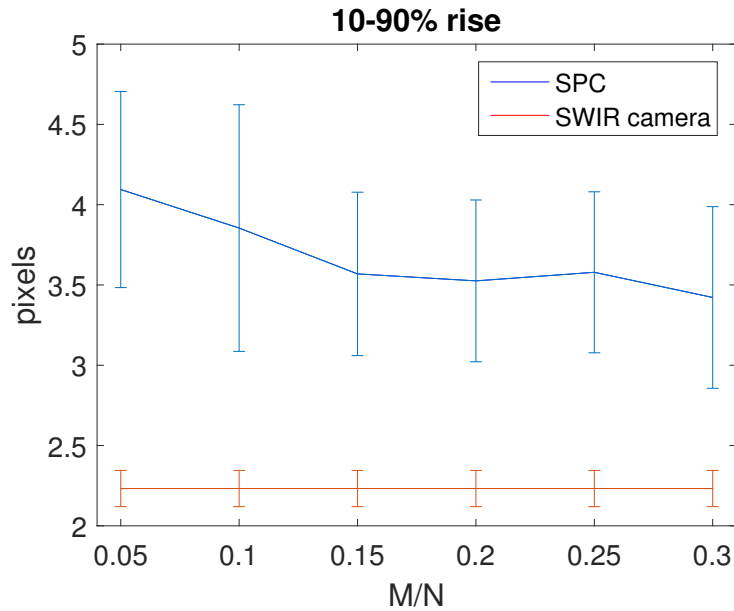


Figure 36: 10-90% rise in pixels.

### 4.3 Luminance change in scene

As predicted in section 3.5.5 dynamics in the scene could result in poor reconstruction performance.

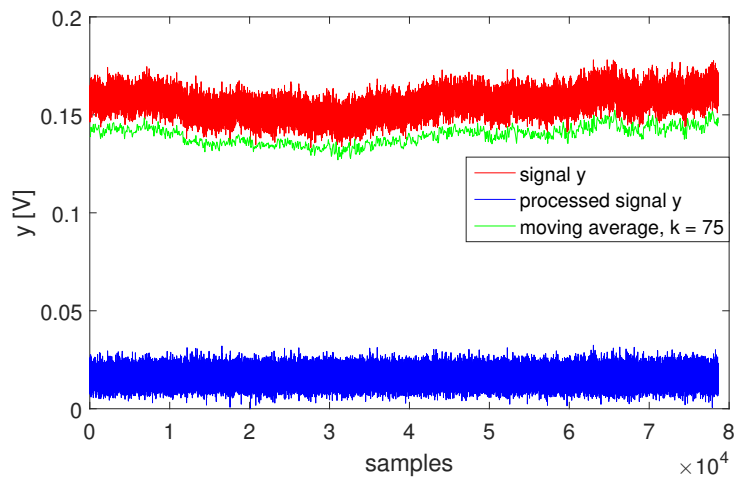


Figure 37: Sampled signal from SPC with light intensity change and the improved moving mean processed signal.

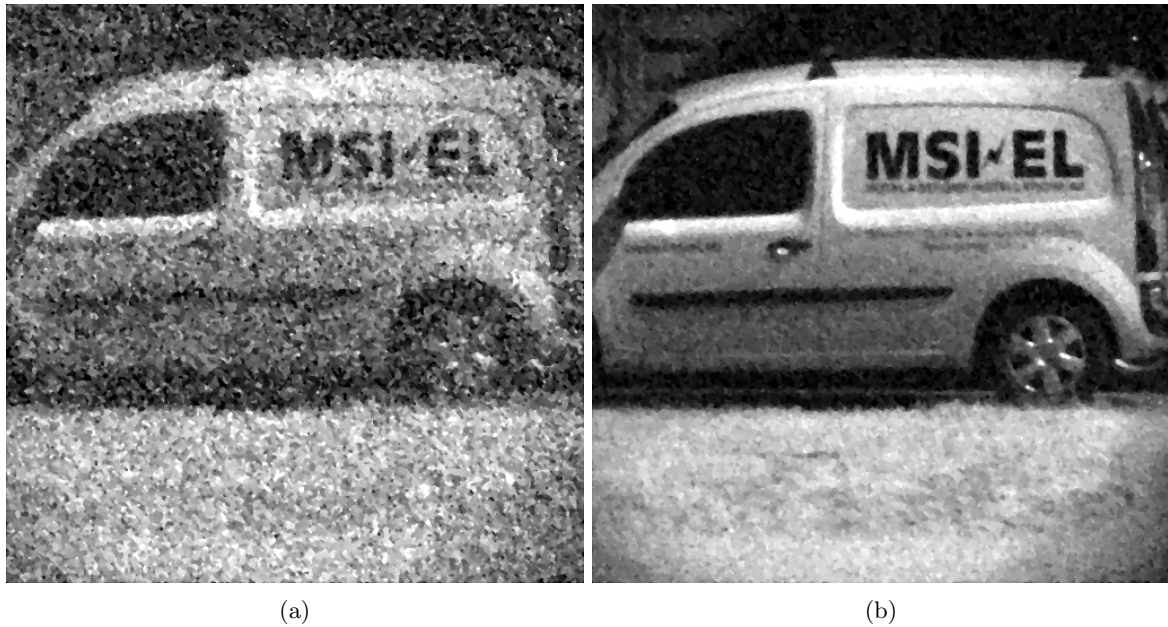


Figure 38: Reconstructed images before and after applying moving mean average.

#### 4.4 Noise analysis

Volt to variance

## References

- [1] G. Y. G. Irina Rish, *Sparse Modeling*. Boca Raton: CRC Press, 2015.
- [2] M. Elad, *Sparse and Redundant Representations*. New York, New York: Springer, 2010.
- [3] D. L. Donoho, “Compressed sensing,” *IEEE Transactions on Information Theory*, vol. 52, no. 4, pp. 1289–1306, Apr. 2006, ISSN: 0018-9448. DOI: 10.1109/TIT.2006.871582.
- [4] D. Takhar, J. N. Laska, M. F. Duarte, K. F. Kelly, R. G. Baraniuk, and M. A. Davenport, “Single-pixel imaging via compressive sampling,” *IEEE Signal Processing Magazine*, vol. 83, 2008.
- [5] R. M. Willett, R. F. Marcia, and J. M. Nichols, “Compressed sensing for optical imaging systems: A tutorial,” *SPIE Optical Engineering*, vol. 50(7), 2011.
- [6] D. Takhar, J. N. Laska, M. B. Wakin, M. F. Duarte, D. Baron, S. Sarvotham, K. F. Kelly, and R. G. Baraniuk, “A new compressive imaging camera architecture using optical-domain compression,” *IS&T/SPIE Computational Imaging*, vol. 5, 2006.
- [7] M. B. Wakin, J. N. Laska, M. F. Duarte, D. Baron, S. Sarvotham, D. Takhar, K. F. Kelly, and R. G. Baraniuk, “An architecture for compressive imaging,” in *IEEE International Conference on Image Processing (ICIP), October 8-11, 2006*, 2006, pp. 1273–1276.
- [8] B. C. L. McMackin M. A. Herman and M. Weldon, “A high-resolution swir camera via compressed sensing,” *SPIE*, vol. 8353, 2012.
- [9] E. Fall, “Compressed sensing for 3d laser radar,” Linköpings University, Master’s thesis, 2014, ISRN: LiTH-ISY-EX-14/4767-SE.
- [10] T. Edeler, K. Olinger, S. Hussmann, and A. Mertins, “Multi image super resolution using compressed sensing,” *ICASSP*, pp. 2868–2871, 2011.
- [11] C. Brännlund and D. Gustafsson, “Single pixel swirl imaging using compressed sensing,” *Symposium on Image Analysis, 14-15 March 2017, Linköping, Sweden*, 2017.
- [12] C. Li, “An efficient algorithm for total variation regularization with applications to the single pixel camera and compressive sensing.,” 2009.
- [13] “Fast compressive sampling with structurally random matrices,” in *2008 IEEE International Conference on Acoustics, Speech and Signal Processing*, Mar. 2008, pp. 3369–3372. DOI: 10.1109/ICASSP.2008.4518373.
- [14] T.T.Do, L. Gan, N. Nguyen, and T. Tran, “Fast and efficient compressive sensing using structurally random matrices,” *IEEE Transactions on Signal Processing*, vol. 60, no. 1, pp. 139–154, Jan. 2012, ISSN: 1053-587X. DOI: 10.1109/TSP.2011.2170977.
- [15] L. Gan, T.T.Do, and T. Tran, “Fast compressive imaging using scrambled block hadamard ensemble,” in *2008 16th European Signal Processing Conference*, Aug. 2008, pp. 1–5.
- [16] C. Zhuoran, Z. Honglin, J. Min, W. Gang, and S. Jingshi, “An improved hadamard measurement matrix based on walsh code for compressive sensing,” in *2013 9th International Conference on Information, Communications Signal Processing*, Dec. 2013, pp. 1–4. DOI: 10.1109/ICICS.2013.6782833.
- [17] S. L. Shishkin, “Fast and robust compressive sensing method using mixed hadamard sensing matrix,” *IEEE Journal on Emerging and Selected Topics in Circuits and Systems*, vol. 2, no. 3, pp. 353–361, Sep. 2012, ISSN: 2156-3357. DOI: 10.1109/JETCAS.2012.2214616.
- [18] A. Bovik, *The Essential Guide to Image Processing*. Elsevier, 2009, ISBN: 978-0-12-374457-9.
- [19] M. Anish, M. Anush Krishna, and B. Alan Conrad, “No-reference image quality assessment in the spatial domain.,” *IEEE TRANSACTIONS ON IMAGE PROCESSING*, vol. 21, pp. 4695–4708, Dec. 2012, ISSN: 1057–7149.

- [20] L. Duval, *50mm fl swirl fixed focal length lens*, Edmund Optics Inc, 2017. [Online]. Available: <https://www.edmundoptics.com/imaging-lenses/fixed-focal-length-lenses/50mm-fl-swirl-fixed-focal-length-lens/> (visited on 05/17/2017).
- [21] *Large area ingaas amplified photodetectors pda20c operation manual*, 1.1, Thorlabs GmbH, Sep. 2016. [Online]. Available: [https://www.thorlabs.com/drawings/e22761fd83df1eab-B1D1D2AA-C921-6D8E-D2B14E11544D8225/PDA20C\\_M-Manual.pdf](https://www.thorlabs.com/drawings/e22761fd83df1eab-B1D1D2AA-C921-6D8E-D2B14E11544D8225/PDA20C_M-Manual.pdf) (visited on 05/16/2017).
- [22] R. Haimi-Cohen and Y. Mark Lai, “Compressive measurements generated by structurally random matrices: Asymptotic normality and quantization.,” *Signal Processing*, vol. 120, pp. 71–87, 2016, ISSN: 0165-1684.